

# AIR QUALITY FORECASTS ON A KILOMETER-SCALE GRID OVER COMPLEX SPANISH TERRAINS

M.T. Pay<sup>1,\*</sup>, F. Martínez<sup>1</sup>, M. Guevara<sup>1</sup>, J.M. Baldasano<sup>1,2</sup>

[1]{Earth Sciences Department, Barcelona Supercomputing Center-Centro Nacional de Supercomputación, Barcelona, Spain}

[2]{Environmental Modeling Laboratory, Technical University of Catalonia, Barcelona, Spain}

[\*]{now at: Laboratoire de Météorologie Dynamique, École Polytechnique, Palaiseau Cedex, France}

## Abstract

CALIOPE-AQFS represents the current state-of-the-art in air quality forecasting systems of high-resolution running on high-performance computing platforms. It provides a 48-h forecast of the main pollutants (NO<sub>2</sub>, O<sub>3</sub>, SO<sub>2</sub>, PM<sub>10</sub>, PM<sub>2.5</sub>, CO, and C<sub>6</sub>H<sub>6</sub>) found at a 4-km horizontal resolution over all of Spain, and at 1 km over the most populated areas in Spain with complex terrains (Barcelona, Madrid and Andalucia domains). Increased horizontal resolution from 4 km to 1 km over the aforementioned domains leads to finer texture and more realistic concentration maps, which is justified by the increase in NO<sub>2</sub>/O<sub>3</sub> spatial correlation coefficients from 0.79/0.69 (4 km) to 0.81/0.73 (1 km). High resolution emissions using the bottom-up HERMESv2.0 model are essential for improving model performance when increasing resolution on an urban scale, but it is still insufficient. Decreasing grid spacing does not reveal the expected improvement in hourly statistics, i.e., decreasing NO<sub>2</sub> bias only by ~2 μgm<sup>-3</sup> and increasing O<sub>3</sub> bias by ~1 μgm<sup>-3</sup>. The grid effect is less pronounced for PM<sub>10</sub> because part of its mass consists of secondary aerosols, which are less affected than the locally emitted primary components by a decreasing grid size. The resolution increase has the highest impact over Barcelona, where air flow is controlled mainly by mesoscale phenomena and a lower PBL. Despite the merits and potential uses of the 1-km simulation, the limitations of current model formulations do not allow confirming their expected superiority close to highly urbanized areas and large sources. Future work should combine high grid resolution with techniques that decrease subgrid variability, and also include models that consider urban morphology and thermal parameters.

## 1 **1 Introduction**

2 The World Health Organization (WHO) has recently shown that there is sufficient  
3 evidence supporting the belief that particulate matter (PM), ozone (O<sub>3</sub>) and nitrogen  
4 dioxide (NO<sub>2</sub>) affect human health (WHO, 2013). Although NO<sub>2</sub> and PM  
5 concentrations improved from 2002 to 2011 in Europe, the situation is still far from  
6 matching the WHO air quality guidelines (AQG). The European annual limit values for  
7 NO<sub>2</sub> (annual) and PM<sub>10</sub> (daily) had been exceeded at 42-43% of the traffic stations in  
8 2011. For the same year, about 33% of the European urban population was exposed to  
9 PM<sub>10</sub> concentration above the daily limit value, and nearly 88% was exposed to the  
10 respective WHO AQG (EEA, 2013). Air pollution legislation for the protection of the  
11 increasing city population has recently increased the demand for urban air pollution  
12 forecasting systems that can assess and understand its dynamics, alert the population  
13 when health-related issues occur, and develop emission abatement plans (EEA, 2011).

14 When applying an air quality modeling system, defining the grid resolution is an  
15 important consideration; the potential benefits of higher-resolution modeling should be  
16 weighed against: the increased complexity of the inputs, CPU time, and disk space  
17 requirements. In theory, higher resolution modeling is expected to yield more accurate  
18 forecasts because of better resolved model input fields (topography, land cover and  
19 emissions), and better mathematical characterization of physical and chemical  
20 processes. Furthermore, high resolutions (ranging from 1 to 5 km) are essential to  
21 reproduce mesoscale phenomena, e.g., those controlling O<sub>3</sub> transport along the  
22 mountainous northeastern Mediterranean coast (Fay and Neunhäuserer, 2006; Jiménez  
23 et al., 2006). Even at the finest scale, the modeled concentrations are not necessarily the  
24 best (Mass et al., 2002; Gego et al., 2005; Valari and Menut, 2008), because increasing  
25 emission and meteorology spatial resolution can also increase uncertainties, at the risk  
26 of reduced model performance. Nowadays, fine horizontal resolution is a persistent  
27 challenge when assessing health impact and population exposure studies (Thompson et  
28 al., 2013).

29 Several studies have evaluated the impact of increasing horizontal resolution on  
30 different scales over the eastern and southeastern USA using the Community Multiscale  
31 Air Quality (CMAQ) model and the Comprehensive Air Quality Model with Extensions  
32 (CAMx), which range from 32 km – 12 km – 4 km (Cohan et al., 2006; Tesche et al.,  
33 2006; Queen and Zhang, 2008). They found no significant changes for O<sub>3</sub> and PM (<5%

1 on average), and those changes were even lower at resolutions of between 12 km and 4  
2 km (<3%). Concerning PM components, [Fountoukis et al. \(2013\)](#) found that increased  
3 resolution provides differences mostly for primary PM rather than secondary PM.  
4 Recently, a model intercomparison exercise, named ScaleDep, was performed to  
5 determine the effect of grid resolution on air quality modeling performance over Europe  
6 at a regional and urban scale ([Cuvelier et al., 2013](#)). The exercise, involving five  
7 Chemical Transport Models (CTMs) (EMEP, CHIMERE, CMAQ, LOTOS-EUROS  
8 and RCGC) running under the same conditions over the full year 2009 and at four  
9 resolutions (56, 28, 14, and 7 km), showed that it is difficult to define a grid size that is  
10 adequate for resolving the urban signal under all conditions affecting Europe. Still, a 14-  
11 km resolution seems to be a good compromise between background applications and  
12 those reproducing most of the urban signals (7 km resolution). However, the ScaleDep  
13 exercise did not distinguish between the different topographies or complex  
14 meteorological patterns which are characteristic of the Iberian Peninsula.

15 Few studies have been performed over selected areas in Spain; and of those, the focus  
16 has been mainly on O<sub>3</sub> and NO<sub>2</sub>. [Vivanco et al. \(2008\)](#) evaluated the annual impact by  
17 increasing the resolution (to 36, 19, and 7 km) over Madrid for NO<sub>2</sub> and O<sub>3</sub>. They used  
18 the WRF-CHIMERE model, disaggregating the EMEP emission inventory based on  
19 land use information. Their evaluation showed that the model improves greatly for NO<sub>2</sub>  
20 than O<sub>3</sub>, and the most significant improvement is achieved when resolution increases  
21 from 36 to 19 km rather than to 7 km, which is linked to increased uncertainty in the  
22 emission data introduced with the disaggregation techniques. [Jiménez et al. \(2006\)](#) used  
23 the MM5-CMAQ model along with a bottom-up emission model (EMICAT2000) to  
24 assess the influence of grid resolution on O<sub>3</sub> (at 8, 4, and 2 km) over the complex terrain  
25 of the northeastern Iberian Peninsula (Catalonia) during a summer pollution episode.  
26 They indicate that, due to improved performance of the mesoscale phenomena and a  
27 better allocation of emissions, a 2-km resolution improves the capability of the model to  
28 simulate exceedances of European limit values. An important issue in both studies is the  
29 emission modeling approach (top-down vs. bottom-up) when applying high resolution  
30 at the local scale (<10 km). As [Fountoukis et al. \(2013\)](#) and [Timmermans et al. \(2013\)](#)  
31 demonstrate, in the range of local scale (e.g., the greater Paris area), the grid resolution  
32 is not currently the major source of discrepancies in model performance; but in fact, the  
33 predicted concentrations and corresponding gradients are more consistent with observed

1 concentrations when provided by bottom-up emission inventories rather than down-  
2 scaled inventories. If local variation in input data (e.g., emission patterns or land use)  
3 cannot be properly characterized, modeling with a finer grid resolution may not provide  
4 any great advantages.

5 Increasing resolution is a technical challenge, since computational cost markedly  
6 increases in inverse proportion to grid spacing. The current progress in computation  
7 allows increased model resolution and for multiple spatial scales to be investigated with  
8 the aim of establishing adequate grid size for forecasting air quality at the local scale.  
9 Recently, [Colette et al. \(2014\)](#) evaluated the impact of increasing resolution up to 2 km  
10 over the European continent by using the CHIMERE model for an episode of air  
11 pollution in 2009. They used 2 million grid cells at over 2000 CPUs of a high  
12 performance computing system, which was hosted by the French Computing Centre for  
13 Research and Technology (CCRT/CEA).

14 In terms of computational resources, horizontal resolution is critical to an operational air  
15 quality forecast. In Europe, operational air quality systems use resolutions of between  
16 12-25 km; meanwhile application to a single country can reach resolutions of between  
17 4-10 km ([Zhang et al., 2012](#)). Over Spain, there are three systems providing air quality  
18 forecasts running at different horizontal resolutions. The lowest resolution system is the  
19 Technical University of Madrid's OPANA (OPERational Atmospheric Numerical model  
20 for urban and regional Areas), running at 27 km x 27 km and based on the  
21 MM5/CMAQ/EMIMO models ([San José et al., 2009](#)). It is followed by the Spanish  
22 meteorological office's system (AEMET,  
23 [http://www.aemet.es/es/eltiempo/prediccion/calidad\\_del\\_aire](http://www.aemet.es/es/eltiempo/prediccion/calidad_del_aire)), which forecasts at 10 km  
24 x 10 km using the HIRLAM-HRN/MOCAGE/GEMS-TNO models. The CALIOPE Air  
25 Quality Forecast System (CALIOPE-AQFS; [Baldasano et al., 2011](#); [Pay et al., 2012a](#);  
26 [and references therein](#)), of the Barcelona Supercomputing Center–Centro Nacional de  
27 Supercomputación (BSC-CNS), runs at the highest resolution, 4 km x 4 km, and it is  
28 based on the WRFv3.5/CMAQv5.0.1/HERMESv2.0/BSC-DREAM8bv2 models.  
29 Moreover, CALIOPE-AQFS provides 1-km x 1-km resolution forecasts for the Madrid  
30 and Barcelona metropolitan areas (since 2009), and the Andalusian region (since 2013).  
31 Such resolution has been possible thanks to both the high performance computing  
32 resources at the BSC-CNS and the availability of detailed emission data covering Spain.

1 The previous works demonstrate there is not a single answer which explains the merits  
2 of high-resolution modeling for all applications. The present work aims to assess the  
3 impact of increasing the horizontal resolution from 4 km to 1 km, specifically over areas  
4 affected by heterogeneous emission patterns and complex terrains such as the Barcelona  
5 and Madrid metropolitan areas (BCN and MAD) together with the Andalusian region  
6 (AND). For that purpose, CALIOPE-AQFS forecasts pollutant concentrations ( $O_3$ ,  $NO_2$ ,  
7 and  $PM_{10}$ ) at two horizontal resolutions: first at a 4-km resolution covering Spain (IP4),  
8 and second at a 1-km resolution covering the AND, BCN, and MAD domains. The  
9 study is performed for the period April 2013, which presented seven days of an air  
10 pollution episode. We use observations from routine air quality monitoring networks to  
11 evaluate both resolutions.

12 Section 2 describes the configuration and computational setup of CALIOPE-AQFS; it  
13 analyses the domains and the period under study and it defines the methodology used to  
14 evaluate the resolution increase. Section 3 quantifies the impact of resolution increase  
15 on forecasting hourly concentrations (and exceedances) in terms of: pollutant, domain,  
16 building density and major emission sources. Section 4 concludes with the main results  
17 and some recommendations.

## 18 **2 Methodology**

### 19 **2.1 Domain and period under study**

20 [Figure 1](#) shows the main  $NO_2$  emission patterns and topographic characteristics of the  
21 domains: the Barcelona and Madrid metropolitan areas (BCN and MAD) and the  
22 Andalusian region (AND). BCN is a coastal area characterized by several valleys  
23 perpendicular to the coastline and two main mountain ranges, one coastal (500 m  
24 height) and one pre-coastal (1000-1700 m height). These features induce mesoscale  
25 phenomena such as sea-breeze and mountain-valley winds. On the other hand, MAD is  
26 a continental region with a much simpler topography that includes the Tajo valley in the  
27 southern of MAD and the mountain range of the Central System located in the  
28 northwestern MAD, with summits reaching 2500 m height. These features bring  
29 different locally-driven flows.

30 The urban contribution in BCN (3.1 million inhabitants) is accompanied by industrial  
31 and power generation emissions, the road network and the harbor; meanwhile the

1 Spanish capital of MAD is mainly influenced by emission from the urban area (5.8  
2 million inhabitants) and the road network that connects MAD with the surrounding  
3 commercial and industrial zones as well as the urban areas.

4 AND is the southern-most region in Spain, with complex topography characterized by  
5 the large depression of the Guadalquivir Basin (delimited by the Iberian Massif and the  
6 Betic Range), which crosses the region from NE to SW over a 60–km stretch. About  
7 three quarters of AND has a mountainous orography, including the Sierra Nevada (3481  
8 m). AND includes one of the five biggest cities in Spain, Seville (~700 000 inhabitants),  
9 which hosts industrial and electric generation activities around the Algeciras bay, and it  
10 is affected by dense maritime traffic through the Strait of Gibraltar.

11 The study is performed over April 2013. At the beginning and end of the month, the  
12 synoptic circulation was controlled by a low pressure system displaced over the south of  
13 the British Isles and which affected Western Europe by leading to atmospheric  
14 instability over the IP. This pattern is typical of transitional months such as April and  
15 November (García-Valero et al., 2012; Valverde et al., 2014), which produce  
16 precipitation and decreased temperatures because of cold and humid winds entering  
17 from the Atlantic Ocean. In contrast, from 12-18 April there was a high pressure system  
18 crossing the Iberian Peninsula in a SW-NE direction, transporting dust from the Sahara  
19 Desert and increased temperatures of up to 25-28°C. During the latter episode,  
20 available air quality stations at the study domains displayed several exceedances of the  
21 European limit values (8 exceedances of the NO<sub>2</sub> hourly limit value, 25 exceedances of  
22 the O<sub>3</sub> information threshold, and 31 exceedances of the PM<sub>10</sub> daily limit value).

## 23 **2.2 CALIOPE-AQFS**

24 CALIOPE-AQFS has provided 48-h air quality forecasts for Europe and Spain since  
25 October 2006 ([www.bsc.es/caliope](http://www.bsc.es/caliope)) and has been described and evaluated in detail  
26 elsewhere (Baldasano et al., 2008, 2011; Pay et al., 2011, 2012a). Briefly, it integrates a  
27 meteorological model (WRF-ARW v3.5; Skamarock and Klemp, 2008), an emission  
28 model (HERMESv2; Guevara et al., 2013), a chemical transport model (CMAQv5.0.1;  
29 Byun and Schere, 2006; Appel et al., 2013), and a mineral dust atmospheric model  
30 (BSC-DREAM8bv2; Pérez et al., 2006; Basart et al., 2012); together, all of these  
31 comprise an air quality forecast system.

1 [Figure 1](#) shows the working domains of CALIOPE-AQFS. First, CALIOPE-AQFS was  
2 run over Europe at a 12-km x 12-km horizontal resolution using initial/boundary  
3 conditions from the Final Analyses of the National Centers of Environmental Prediction  
4 (FNL/NCEP). The analyses began at 12 h UTC, at intervals of 6 h (0.5°x0.5°) for  
5 meteorology. The global model LMDz-INCA2 (3.75°x2.5°, [Szopa et al., 2009](#)) was used  
6 for chemistry. Then, CALIOPE-AQFS was run at a higher horizontal resolution (4 km x  
7 4 km (IP4)) over the Iberian Peninsula using one-way nesting. In the present work  
8 CALIOPE-AQFS runs at 1 km x 1 km over the domains at hand (AND, BCN and  
9 MAD), with nesting of over IP4 throughout. HERMESv2.0 forecasts anthropogenic  
10 emissions for the year 2009 by following a bottom-up methodology (point, linear and  
11 area), and biogenic emissions using the MEGANv2.0.4 model ([Guenther et al., 2006](#)).  
12 Emissions are aggregated into 1-km grids for AND, BCN and MAD 1-km simulations,  
13 and into 4 km for IP4.

14 Vertically, WRF-ARW is configured with 38 sigma layers up to 50 hPa, with 11  
15 characterizing the planetary boundary layer (PBL); meanwhile CMAQ vertical levels  
16 are obtained by collapsing from the 38 WRF levels to a total of 15 layers that steadily  
17 increase from the surface up to 50 hPa. Six layers are within the PBL, and the first layer  
18 depth is 39 m.

19 The present WRF setup uses: the Rapid Radiation Transfer Model (RRTM) and Dudhia  
20 for long- and short-wave radiation, respectively; the Kain-Fritsch cumulus  
21 parameterization ([Kain and Fritsch, 1990](#)); the single-moment 3-class (WSM3)  
22 microphysics scheme; and the Yonsei University PBL scheme (YSU). The Noah land-  
23 surface model (NoahLSM), based on the U.S. Geological Survey's (USGS) land-use  
24 data, is used by default in the present WRF configuration.

25 Currently, a new CMAQ version is being tested in the CMAS community, namely  
26 CMAQv5.0 ([CMAQ, 2012](#)). It includes substantial scientific improvements over  
27 Version 4.5 and is especially devoted to improving SOA formation as well as the  
28 dynamic interactions of fine and coarse aerosols. Based on the evaluation results from  
29 the previous CMAQ version within CALIOPE-AQFS (4.5 vs. 5.0) ([Pay et al. 2012b](#)),  
30 CMAQ has been updated to Version 5.0.1 using the CB05 chemical mechanism  
31 ([Yarwood et al., 2005](#)), the AERO5 for aerosol modeling, and the in-line photolysis  
32 calculation.



1 CALIOPE-AQFS considers desert dust contribution by means of the BSC-  
2 DREAM8bv2, which runs off-line at a  $0.5^\circ \times 0.5^\circ$  resolution covering Europe, North  
3 Africa and the Middle East. Its outputs are mass conservative interpolated to the  
4 CMAQ's Lambert conformal conic grids and at the required resolution and domain.  
5 After interpolating, the modeled  $PM_{10}$  concentration is: the sum of Aitken,  
6 accumulation and coarse-mode modes from CMAQ, and the corresponding BSC-  
7 DREAM8bv2 bins with a diameter of  $\leq 10 \mu m$  (Pay et al., 2012a).

### 8 **2.3 Computational strategy**

9 Running CALIOPE-AQFS at 4 and 1 km is a technical challenge. The simulations are  
10 run on MareNostrum supercomputer (Intel Xeon E5-2670, 16 CPUs and 64 GB RAM  
11 memory per node) at BSC-CNS. Table 1 depicts the computational requirements for  
12 forecasting air quality at 48 h for each domain. The number of CPUs was chosen to  
13 maximize CPU efficiency. Thanks to the parallelization of meteorological and air  
14 quality models, MareNostrum uses up to 256 CPUs. Due to the variable nature and  
15 complex dependencies, the computational time for forecasting 48 h of air quality fields  
16 for the 4 domains is 8-9 hours. The most computationally demanding domain is the  
17 AND, at 1-km resolution (366x358 cells, 256 CPU max., and 300 min). For the April  
18 2013 simulation, times add up to 2880 CPU hours/day, or 86400 CPU hours in one CPU  
19 (9.86 years). The storage for the April 2013 output files was 6.13 TB (~200 GB/day).

### 20 **2.4 Evaluating the increase in resolution**

21 Comparing CALIOPE-AQFS grid resolutions and measurements was done in terms of  
22 gas-phase and aerosol concentrations ( $O_3$ ,  $NO_2$ , and  $PM_{10}$ ). Representativeness continue  
23 to be a challenge when comparing gridded simulations to observational data at a point  
24 in time and space, as modeled concentrations represent a volumetric average over an  
25 entire grid cell. Furthermore, the stochastic compound embedded in the observations is  
26 not accounted for. Concerning temporal representativeness in the present comparison,  
27 both modeled and measured concentrations are averaged hourly. CALIOPE-AQFS  
28 operationally receives air quality measurements from Spanish administrative networks  
29 in near real time (NRT) without any quality data or quality control. For the present  
30 study, NRT measurements are filtered by removing data before and after measurement  
31 interruptions or calibrations. Also, a minimum cut-off threshold of  $1 \mu g m^{-3}$  is applied to



1 the observed concentrations in order to avoid unrealistic observations. After filtering,  
2 the number of stations is 48/30/36 for O<sub>3</sub>, 51/42/42 for NO<sub>2</sub>, and 52/15/33 for PM<sub>10</sub> at  
3 AND/BCN/MAD.

4 The meteorological fields are evaluated for wind speed at 10 m (U10), and wind  
5 direction (WD10) and temperature at 2 m (T2M), all of them at 10 METAR stations  
6 located at airports (6/2/2 stations in AND/BCN/MAD). They are discussed in [Sect. S1](#).

7 [Figure 2](#) shows the location of the air quality and METAR (METeorological Aerodrome  
8 Report) stations over the respective domains. The spatial representativeness of the air  
9 quality network is highly variable. The influence of the station type is based on two  
10 classifications of air quality monitoring stations, the environment type (rural, R;  
11 suburban, S; and urban, U), and the dominant emission source (traffic, T; industrial, I;  
12 and background, B). These were derived from the Council decision 97/100/EC ([Garber  
13 et al. 2002](#)).

14 The evaluation is based on discrete statistics performed on an hourly basis. We consider  
15 the correlation coefficient (r), mean (absolute, relative, and fractional) biases (MB,  
16 MNBE, and MFB), and error (MAE, MNGE, and MFE). Root Mean Square Error  
17 (RMSE) is also calculated because it intensifies large differences between measured and  
18 observed concentrations (Table A1).

19 In order to evaluate the effect of resolution increase on forecasted exceedances and non-  
20 exceedances of limit values established by the European legislation, we calculate  
21 categorical statistics based on comparisons with fixed concentration thresholds (T). The  
22 calculated statistics are accuracy (A), bias (B), probability of detection (POD), critical  
23 success index (CSI), and false alarm ratio (FAR), whose formulas and descriptions are  
24 explained in Table A2 and elsewhere in [Kang et al. \(2005\)](#) and [Eder et al. \(2006\)](#). The  
25 2008/50/EC directive sets an information threshold of 180 µgm<sup>-3</sup> for maximum daily O<sub>3</sub>  
26 concentrations (Max 1h O<sub>3</sub>) and a target value of 120 µgm<sup>-3</sup> for the maximum daily 8-h  
27 running O<sub>3</sub> mean (Max 8h O<sub>3</sub>), which should not be exceeded more than 25 days per  
28 year. It establishes a limit value of 200 µgm<sup>-3</sup> for maximum daily NO<sub>2</sub> concentrations  
29 (Max 1h NO<sub>2</sub>), and 50 µgm<sup>-3</sup> for the daily PM<sub>10</sub> mean (Mean 24h PM<sub>10</sub>), which should  
30 not be exceeded more than 35 times per year. Therefore, categorical evaluation will be  
31 performed for Max 1h NO<sub>2</sub>, Max 1h and Max 8h O<sub>3</sub>, and Mean 24h PM<sub>10</sub>. Note that  
32 mean and maximum concentrations are calculated by considering at least 75% of the

1 data in the corresponding time base, i.e., values of at least 18 hours per day for Mean 24  
2 h, Max 1h, and Max 8h; and 6 hours for 8 h values, as established by 2008/50/EC.

### 3 **3 Concentration maps and spatial representativeness**

4 To analyze the spatial differences between resolutions, [Figs. 3, 4, and 5](#) show the  
5 monthly mean concentration maps for April 2013 over MAD, BCN and AND domains  
6 at 4 km (left panels) and 1 km (right panels) for NO<sub>2</sub>, O<sub>3</sub>, and PM<sub>10</sub>, respectively.

7 The maps of NO<sub>2</sub> and PM<sub>10</sub> at both resolutions display similar distribution along the  
8 MAD and BCN urban plumes. On-road traffic constitutes the main source of primary  
9 pollutants in MAD and BCN. HERMESv2.0 estimates that 75% and 59% of NO<sub>x</sub>  
10 emissions are produced by on-road traffic in both domains, respectively. Consequently,  
11 when the resolution increases, the monthly mean O<sub>3</sub> concentration maps are almost  
12 identical, although the NO<sub>x</sub> titration effect on O<sub>3</sub> is significant along highways and  
13 major point sources. In AND, NO<sub>2</sub> and O<sub>3</sub> concentrations are also conserved between  
14 resolutions along the shipping route crossing the Strait of Gibraltar towards the  
15 Mediterranean Sea.

16 However, the definition of NO<sub>2</sub> concentrations along highways connecting the biggest  
17 cities with the rest of the country and industrial sectors are more easily identified at 1-  
18 km simulations than at 4 km, especially along those roads from/to Barcelona (e.g., the  
19 AP7 Mediterranean highway and C32, which connects the harbor and the airport) and  
20 Madrid (the A-2 and A-6 in the north, and A-3, A-4 and A-5 in the south). In the same  
21 way, 1-km O<sub>3</sub> maps are more textured than those at 4 km along highways, because the  
22 titration effect is more significant at 1 km, due to less dilution within grid cells. The  
23 titration effect of NO<sub>x</sub> on O<sub>3</sub> over the main sources is more forceful in BCN than in  
24 MAD, given that BCN has a larger concentration gradient resulting from complex  
25 topography and recirculation flows that accumulate pollutants.

26 The improvement of the definition along roads in AND is lower than that observed in  
27 the MAD and BCN domains, due to the fact that the AND domain is bigger and  
28 displays lower traffic emission sources than the MAD or BCN domains. Regarding  
29 PM<sub>10</sub>, the main component in AND is the desert dust (~40% in both resolutions) from  
30 North Africa. This is because there were two episodes on 14-19th and 25-26th April that  
31 affected the IP, as shown by the S-N PM<sub>10</sub> gradient ([Fig.5e and f](#)). The desert dust is  
32 transported from long-range simulation with BSC-DREAM8bv2.

1 Over complex terrains, the 1-km simulation allows reproducing more realistic NO<sub>2</sub>  
2 concentration maps because of its more detailed topographic information input. For  
3 instance, the BCN 1-km simulation displays the lowest NO<sub>2</sub> concentrations (< 10 µgm<sup>-3</sup>)  
4 along the coastal chain (500 m height) and pre-coastal chain (1000-1700 m height),  
5 except for the city's urban hill, where concentrations reach 20-40 µgm<sup>-3</sup>. In contrast, the  
6 4-km simulation provides smoother NO<sub>2</sub> concentrations without any concentration  
7 gradient. Thus, the 1-km simulation generates slightly higher O<sub>3</sub> background  
8 concentrations than does the 4-km simulation along the BCN pre-coastal chain (66-70  
9 vs. 70-74 µgm<sup>-3</sup>), as well as across the Iberian Massif (AND), where the O<sub>3</sub> map  
10 displays significant structure due to the higher resolution topography that shapes the  
11 basin and the on-road traffic.

12 [Figures 3, 4, and 5](#) include dots corresponding to mean concentrations at air quality  
13 stations that help to qualitatively evaluate the modeled spatial representativeness at both  
14 resolutions. Note the high concordance between NO<sub>2</sub> observations and the 1-km  
15 simulation near the primary suburban traffic roads in BCN (e.g., Vilafranca, Igualada,  
16 Manresa, and Mataró). Regarding O<sub>3</sub>, although observed concentrations depict an  
17 overall tendency of the model to underestimate concentrations at both resolutions, the 1-  
18 km simulation displays a higher accord with measurements at rural background stations  
19 (e.g., El Atazar, San Martín, Villa de Prado, Villarejo and Orosco stations in MAD), and  
20 at suburban traffic stations (e.g., Manresa, Igualada and Vilafranca in BCN, with  
21 modeled O<sub>3</sub> concentrations of around 54-58 µgm<sup>-3</sup> at 1 km, and 60-66 µgm<sup>-3</sup> at 4 km).  
22 For PM<sub>10</sub>, comparisons with measurements show that modeled concentrations are  
23 underestimated over background areas, mainly outside the urban/suburban area, as  
24 already discussed in [Pay et al. \(2012a\)](#). However, PM<sub>10</sub> measurements at the  
25 urban/suburban stations of Vilafranca, Sant Celoni, and Mataró in BCN (14-16 µgm<sup>-3</sup>)  
26 show a higher concordance at 1 km than at 4 km (12-14 µgm<sup>-3</sup> vs. 8-10 µgm<sup>-3</sup>).

27 The spatial variability of the increased resolution is quantitatively analyzed by means of  
28 concentration maps, shown in [Fig. 6](#) for NO<sub>2</sub>, O<sub>3</sub> and PM<sub>10</sub> over AND, BCN and MAD.  
29 Over all domains, the explained spatial variability improves as a function of the  
30 resolution increase for NO<sub>2</sub> and O<sub>3</sub>, which is sustained by the increase in monthly r  
31 from 0.79 (4 km) to 0.81 (1 km) for NO<sub>2</sub>, and from 0.69 to 0.73 for O<sub>3</sub>. The slopes  
32 improve with the resolution increase, from 0.72 (4 km) to 0.77 (1 km) for NO<sub>2</sub>, and  
33 from 0.50 (4 km) to 0.54 (1 km) for O<sub>3</sub>. This results from the improved model

1 performance at urban stations, indicating that CALIOPE-AQFS explains better the  
2 magnitude of the variability between urban regions at 1 km than at 4 km. In contrast, for  
3 PM<sub>10</sub>, the monthly  $r$  decreases from 0.67 to 0.58 when the resolution increases.  
4 Although the PM<sub>10</sub> spatial variability over BCN and MAD improves when the  
5 resolution increases ( $r$  increases by 0.01 and 0.04, respectively), the global correlation  
6 coefficient deviates mainly at the AND stations (52/100), where  $r$  decreases by 0.1 from  
7 0.36 (4 km) to 0.26 (1 km). Despite the unfavorable effect of the resolution increase in  
8 PM<sub>10</sub> over AND, the NO<sub>2</sub> and O<sub>3</sub> concentrations show the highest absolute increase in  
9 the spatial  $r$  over this domain, from 0.62 (4 km) to 0.71 (1 km) for NO<sub>2</sub> and from 0.58 (4  
10 km) to 0.64 (1 km) for O<sub>3</sub> (increasing  $r$  by 0.09 and 0.06, respectively).

## 11 **4 Temporal evaluation**

12 The present section discusses the temporal evaluation of the resolution increase by  
13 pollutant, environment, predominant emission sources, and study domain. [Fig. 7](#)  
14 summarizes the statistical evaluation.

### 15 **4.1 Pollutant**

16 [Table 2](#) depicts the statistical evaluation by pollutant, with a focus on the reproduction  
17 of high concentrations established by the European directive (2008/50/EC). Depending  
18 on the pollutant's lifetime and variability, as well as its dependency on precursors,  
19 increased resolution shows different impacts. The resolution increase has a positive  
20 effect on NO<sub>2</sub>, decreasing its bias by 2.0  $\mu\text{g m}^{-3}$  (from -4.5 to -2.5  $\mu\text{g m}^{-3}$ ); but it also  
21 increases absolute (squared) errors by 0.3  $\mu\text{g m}^{-3}$  (0.9  $\mu\text{g m}^{-3}$ ). This positive effect is  
22 sustained by the perceptual variability, where the MB (MFB) is reduced by 42% (19%);  
23 whereas MAE (MFE) only increases by 2% (1%). The correlation coefficient does not  
24 significantly change, which is obvious because emissions at both resolutions are  
25 modeled using the same approach. The bias improvement at 1-km resolution is justified,  
26 because the higher resolution leads to better emission allocation from point, linear or  
27 area sources; it decreases the artificial dilution of emission compared to the larger grid  
28 area; and, due to the decrease of artificial dilution, it treats chemistry more properly near  
29 large emission sources.

30 In contrast, the resolution increase has a negative effect on hourly and Max 8h O<sub>3</sub>  
31 concentrations because it increases biases and errors by 0.1-0.8  $\mu\text{g m}^{-3}$ . Relative  
32 (fractional) biases and errors increase by 8% (15%) and 1% (1%), respectively, for

1 hourly O<sub>3</sub>; and 6% and 4% for Max 1h O<sub>3</sub>. However, the statistical evaluation alone is  
2 not enough to explain the impact of the resolution increase on O<sub>3</sub> concentrations.

3 According to the categorical evaluation, only a few exceedances of the European target  
4 and limit values were detected for Max 1h NO<sub>2</sub> (9), Max 1h O<sub>3</sub> (25), and Mean 24h PM<sub>10</sub>  
5 (31) in April 2013. Thus, categorical evaluation is performed on the temporal basis  
6 established by the European legislation, but it uses a T based on the 75p of the observed  
7 concentrations in each case. T corresponds to 71 μgm<sup>-3</sup> for Max 1h NO<sub>2</sub>, 108 (101)  
8 μgm<sup>-3</sup> for Max 1h (Max 8h) O<sub>3</sub>, and 27 μgm<sup>-3</sup> for Mean 24h PM<sub>10</sub>.

9 Overall, CALIOPE-AQFS underestimates exceedances at both resolutions, indicating  
10 that errors of missing observed exceedances are not totally resolved by a resolution  
11 increase (a<d). The best performance is found for Max 1h NO<sub>2</sub>, where bias (B)  
12 improves from 37% (4 km) to 40% (1 km).

13 For NO<sub>2</sub> Max 1h, there are 953 observed exceedances (b+d) of the threshold (T=47  
14 μgm<sup>-3</sup>). Increasing the resolution increases the POD from 49% (4 km) to 56% (1 km).  
15 As POD, CSI studies the exceedances, but in a more coherent way by considering both  
16 false alarms and missing events. Both POD and CSI increase by 14% and 20% when  
17 resolution is increased. The opposite effect appears for O<sub>3</sub>. Aside from the fact that the  
18 O<sub>3</sub> POD is relatively low, the POD decreases as the resolution increases. Of the 1306  
19 observed exceedances of the 108 μgm<sup>-3</sup> Max 1h, CALIOPE-AQFS detected 112  
20 exceedances at 4 km and only 96 at 1 km. Increasing resolution decreases POD and CSI  
21 by 22% and 25% for O<sub>3</sub> Max 1h, whereas they do not significantly change for Max 8h  
22 O<sub>3</sub> and Mean 24h PM<sub>10</sub>.

23 FAR increases for Max 1h NO<sub>2</sub> (from 40% to 42%) and decreases for Max 1h O<sub>3</sub> (from  
24 27% to 17%) when the resolution increases. In relative terms, this variability is more  
25 significant for Max 1h O<sub>3</sub> (37 %) than for Max 1h NO<sub>2</sub> (5%), indicating that, in terms of  
26 failures, the resolution has a positive global effect by reducing false exceedances.

27 For various reasons, accuracy (A) remains almost constant when the resolution  
28 increases. Regarding NO<sub>2</sub> and O<sub>3</sub>, it is due to a stable sum of b and c, increasing the b at  
29 the cost of c, and vice versa. For NO<sub>2</sub>, the number of hits (b) to forecast Max 1h at 1  
30 km is higher than 4 km (537 vs. 466), but the number of correct negatives at 1 km is

1 lower than at 4 km (2439 vs. 2517). The resolution increase has the opposite effect on  
2 O<sub>3</sub> over b and c for both Max 1h and Max 8h.

### 3 **4.2 PM<sub>10</sub> components**

4 The resolution increase has the lowest effect on PM<sub>10</sub> hourly concentrations and its  
5 exceedances (<1%). PM<sub>10</sub> components are secondary inorganic aerosols (SIA), which  
6 include sulfate (SO<sub>4</sub>), nitrate (NO<sub>3</sub>) ammonium (NH<sub>4</sub>), secondary organic aerosol  
7 (SOA), elemental carbon (EC), sea salt (SS), desert dust (DD), and primary PM (PPM).

8 [Pay et al. \(2012a\)](#) already evaluated the PM components at some Spanish urban and  
9 rural background stations using the CALIOPE-AQFS based on CMAQv4.5, and they  
10 showed that the model underestimated the secondary inorganic aerosols by a factor of 2-  
11 3. The highest underestimation was found for fine carbonaceous aerosols (a factor of 4),  
12 in part related to the state-of-the-science concerning secondary organic aerosol  
13 formation pathways. The updated version of CMAQ, v5.0.1 includes scientific  
14 improvements concerning SOA formation and aerosol dynamics, which could improve  
15 the modeled PM<sub>10</sub> performance for its components.

16 [Figure 8a](#) shows that the resolution increase does not significantly change the PM<sub>10</sub>  
17 composition. DD remains the main contributor (~40-41%), followed by PPM (22-24%),  
18 SIA (~21-22%), SS (9-11%), EC (~4%) and SOA (~0.6%). However, the effect of the  
19 increased resolution on PM<sub>10</sub> component concentrations is different ([Fig. 8b](#)),  
20 depending on their origin, atmospheric cycle and the way they are modeled. DD  
21 concentrations do not change between resolutions, because they are mass conservative  
22 when interpolated from 0.5°x0.5° till 1 km x 1 km.

23 Regarding SIA, increasing the resolution increases NO<sub>3</sub> and NH<sub>4</sub> concentrations by 4  
24 and ~2%, respectively, and it decreases SO<sub>4</sub> by ~2%. The NH<sub>4</sub> increase means there are  
25 more primary precursors (H<sub>2</sub>SO<sub>4</sub> or HNO<sub>3</sub>/NO<sub>2</sub>) available to neutralize NH<sub>3</sub> (gas) to  
26 NH<sub>4</sub> (aerosol). However, the variability between SO<sub>4</sub> and NO<sub>3</sub> is more difficult to  
27 explain, due to the nonlinearity of photochemistry and aerosol formation, which is  
28 controlled to some extent by the ISORROPIA thermodynamic equilibrium.  
29 Furthermore, the absence of aerosol measurements for April 2013 does not allow us to  
30 explain this situation.

1 The resolution increase displays the highest decrease for SS (~16%). CMAQv5.0.1  
2 simulates SS emission as a function of the wind speed and the relative humidity (Gong,  
3 2003; Zhang et al., 2005). Although not shown here, when the resolution increases, the  
4 wind speed increases at the available PM<sub>10</sub> stations by ~1.4/0.4/0.2 ms<sup>-1</sup> over  
5 AND/BCN/ MAD, and also over the open ocean.

6 For primary PM components (EC and PPM), increasing resolution presents the highest  
7 increase in concentration (by 10 and ~12%, respectively). As for NO<sub>2</sub>, the 1-km  
8 simulation leads to a reduced effect of artificial dilution of emissions in a grid cell, so  
9 concentration gradients are stronger than in the 4-km simulation.

### 10 **4.3 Domain**

11 Due to differences in geographical location and emission patterns over the domains  
12 under study, the resolution increase has different impacts (Fig. 7). BCN shows the  
13 highest NO<sub>2</sub> bias decrease (73%) when the resolution increases, yet with no effect on  
14 the correlation (<7%). However, O<sub>3</sub> shows significant variability over BCN, increasing  
15 r (by 4%) and MB (by 23%). To a lesser extent, MB also increases over AND (by 8%).  
16 Meanwhile, the variability over MAD is reduced (<4%). MB decreases for PM<sub>10</sub> (< 1  
17 μgm<sup>-3</sup>) over the urban domains of MAD (3%) and BCN (16%), and increases over AND  
18 (7%).

19 Figure 9 analyzes the impact of the resolution increase on daily cycles. Although PBL  
20 measurements are not available, PBL daily cycles are displayed together in order to find  
21 some correlations with the daily pollutant variability. Due to the lamination of PBL  
22 growth by the Mediterranean sea breezes, the PBL reaches its maximum height at  
23 midday, being the highest in MAD (1600 m AGL) followed by AND (1000 m AGL)  
24 and BCN (900 m AGL).

25 As shown in Sect. S1, the pollutant transport at the BCN coastal domain is controlled by  
26 mesoscale phenomena such as sea-breezes (day) and land-breezes (night), which are a  
27 result of its complex topography and location (Baldasano et al., 1994; Millán et al.,  
28 1997; Gonçalves et al., 2009). The NO<sub>2</sub> daily cycle is highly influenced by traffic  
29 emissions (Fig. 9). Both resolutions show the highest underestimations at the morning  
30 peak (5-9 am) (~20 μgm<sup>-3</sup>). Although the afternoon peak is well reproduced, there is  
31 excessive variability at both resolutions, which results from problems with wind



1 direction. During the sea breeze period, the mean simulated wind was more easterly  
2 than westerly, as registered by measurements (Sect. S1). Several works indicate that  
3 WRF does not faithfully reproduce the morning and evening transition over the urban  
4 environment, possibly because it does not model the heat retention in cities (Makar et  
5 al., 2006; Appel et al., 2013). Increasing the resolution increases the NO<sub>2</sub> concentrations  
6 from 14 μgm<sup>-3</sup> (4 km) to 17 μgm<sup>-3</sup> (1 km) during the morning hours after sunrise (5-9  
7 am) and in the evening hours after sunset (5-9 pm). This behavior could be explained by  
8 PBL variability when increasing the resolution, which decreases PBL height by ~33 m  
9 for these hours.

10 NO<sub>2</sub> performance impacts the O<sub>3</sub> daily cycles over BCN, showing that 4- and 1-km  
11 simulations underestimate maximum O<sub>3</sub> concentrations by ~20 μgm<sup>-3</sup> at midday (1-4  
12 pm), and it overestimates minimum O<sub>3</sub> concentration by ~20 μgm<sup>-3</sup> in the morning  
13 hours after sunrise (5-9 am). The resolution increase allows slightly decreasing O<sub>3</sub>  
14 concentrations at night, which is perhaps controlled by the PBL decreasing at 1 km  
15 during the early morning and late afternoon, when PBL reaches the minimum height.  
16 During these hours, the titration effect of NO<sub>2</sub> on O<sub>3</sub> is more effective, improving the O<sub>3</sub>  
17 overestimation of the daily minimum, which allows a slightly increasing hourly r (2%).  
18 However, O<sub>3</sub> underestimation increases in the late afternoon, contributing to an increase  
19 in the hourly mean bias from ~9 μgm<sup>-3</sup> (4 km) to ~11 μgm<sup>-3</sup> (1 km).

20 In BCN, the PM<sub>10</sub> underestimation is not systematic throughout the daily cycle (Fig. 9),  
21 which shows a bias of ~20/10 μgm<sup>-3</sup> at day/night time. The higher daytime  
22 underestimation as compared to the nighttime cannot be explained by the current  
23 results, but it could be a result of missing sources and problems with PBL  
24 overestimation and emission dilutions. The resolution increase allows reducing the bias  
25 by ~1 μgm<sup>-3</sup> (16%), especially during early morning and late afternoon, when the  
26 highest PBL variability between resolutions is detected. Although the evaluation of  
27 T2M, U10 and WD10 indicates that the resolution increase has a low effect over BCN  
28 (Sect. S1), the reduction of the artificial dilution of NO<sub>2</sub> emissions –together with a  
29 lower PBL height at 1 km than at 4 km during the night and early morning– allows  
30 improving NO<sub>2</sub>, O<sub>3</sub> and PM<sub>10</sub> concentrations, which in turn decreases their biases.

31 In AND, the model at both resolutions underestimates observed NO<sub>2</sub> concentrations  
32 throughout the daily cycle (~5 μgm<sup>-3</sup>), with the highest underestimation at the morning

1 peak ( $\sim 25 \mu\text{gm}^{-3}$ ) and the lowest at the afternoon peak ( $\sim 10 \mu\text{gm}^{-3}$ ). The resolution  
2 increase reduces the bias from  $-3.5$  to  $2 \mu\text{gm}^{-3}$  (by 43%) and increases  $r$  by 7% (from  
3  $0.39$  to  $0.41$ ). As in BCN, the  $\text{NO}_2$  underestimation directly impacts the  $\text{O}_3$  daily cycle  
4 (which the resolution increase cannot resolve), increasing the bias by  $\sim 1 \mu\text{gm}^{-3}$ , a  
5 phenomenon that is predominant in the morning hours. In the case of  $\text{PM}_{10}$ , the daily  
6 cycle indicates that the biases are almost systematic throughout the daily cycle ( $\sim 22$   
7  $\mu\text{gm}^{-3}$ ). Increasing the resolution increases the bias by less than 4% in the late  
8 afternoon, which is perhaps dominated by the PBL decrease. When the resolution is  
9 increased,  $\text{NO}_2$  performs better because of the improved model performance for the  
10 temperature and wind speed (Sect. S1), as well as the lower nocturnal and higher diurnal  
11 PBL. Meanwhile the  $\text{O}_3$  and  $\text{PM}_{10}$  performance do not significantly change.

12 During April 2013, the main flow over MAD was controlled by S-SW synoptic winds  
13 channeled by orographic barriers in the NW domain and the Tajo valley (Valverde et  
14 al., 2014). The  $\text{NO}_2$  daily cycle depicts a high influence of traffic emissions (Fig. 9),  
15 showing significant model underestimation at both resolutions for the  
16 morning/afternoon peaks ( $\sim 15/10 \mu\text{gm}^{-3}$ ). Note that, in terms of mean and variability  
17 resulting from southeastern winds, the model performs well at the afternoon peak.  $\text{NO}_2$   
18 performance leads to more accurate  $\text{O}_3$  daily cycles than in AND and BCN, especially  
19 in the early morning, when the titration effect of  $\text{NO}_2$  is more efficient because the  $\text{NO}_2$   
20 morning peak underestimation is lower when compared to the other domains.  
21 Meanwhile, the modeled  $\text{PM}_{10}$  at both resolutions presents a profile controlled by traffic  
22 emissions. Observed concentrations display a flatter daily cycle, in which the model  
23 underestimation reaches  $40 \mu\text{gm}^{-3}$  in the morning. Increasing resolution shows a  
24 positive effect for  $\text{NO}_2$ , and  $\text{PM}_{10}$  increases  $r$  by  $0.01$  and reduces MB and RMSE by  
25  $0.1$ - $0.2 \mu\text{gm}^{-3}$ . However, it depicts the lowest variability when compared to the other  
26 domains ( $<5\%$  for bias, error and  $r$ ), which is the result of a relatively simpler  
27 topography and meteorological patterns.

#### 28 **4.4 Environment and major sources**

29 Figure 7 shows that the resolution impact also depends on the type of area and the  
30 dominant emission source. Theoretically, the meteorological fields of urban areas differ  
31 from those of surrounding rural areas because of their different morphology (radiation

1 trapping and wind profiles), surface materials (heat storage) and variable energy  
2 consumption (heat release).

3 Increasing resolution reduces the NO<sub>2</sub> bias at suburban and urban stations by 1.8-2 μgm<sup>-3</sup>  
4 <sup>3</sup>, and, to a lesser extent, by 1.2 μgm<sup>-3</sup> at rural stations. The correlation coefficients also  
5 improve at suburban stations (from 0.48 to 0.52) and rural stations (from 0.34 to 0.35).  
6 That is not surprising, because the 1-km grid allows better allocation of land-use  
7 categories (urban vs. rural) and of their fraction in a grid cell than does a 4-km grid. The  
8 NO<sub>2</sub> biases exhibit a relative 39% (65%) decrease at urban (background) stations, but  
9 O<sub>3</sub> biases increase by 9% (5%). For PM<sub>10</sub>, the resolution increase does not significantly  
10 change as a function of area type, and it depicts variation in biases and errors of less  
11 than ±4% (<0.5 μgm<sup>-3</sup>).

12 The low improvement at urban stations is obviously because the NoahLSM land-surface  
13 model does not consider the effect of urban morphology or thermal parameters in order  
14 to accurately model meteorological fields. Modeling air quality on an urban scale over  
15 cities requires a description of the heat/momentum exchange between buildings and the  
16 lower atmospheric layers. For instance, the impact of using an urban model on  
17 meteorological fields over the greater Paris area was studied by [Kim et al. \(2013\)](#) using  
18 WRF with the Urban Canopy Model, demonstrating that, below a 1000-m height,  
19 overestimations of wind speed were significantly reduced.

20 The effect of increasing resolution is positive for primary pollutants near important  
21 emission sources. For example, it reduces NO<sub>2</sub> biases at traffic (industrial) stations by  
22 ~3 μgm<sup>-3</sup> (2 μgm<sup>-3</sup>), but it increases O<sub>3</sub> biases by ~2 μgm<sup>-3</sup> (1 μgm<sup>-3</sup>). However, the  
23 resolution increase in the range of 4-1 km does not exhibit the expected improvement  
24 on the hourly statistics that are based on the constraints of the current model  
25 formulation. In other words, it cannot resolve the subgrid air quality variability merely  
26 by increasing resolution. For instance, although on-road traffic emissions are estimated  
27 by following a bottom-up approach along highways and routes, heterogeneity is lost in  
28 the CTM volume averaging process, which artificially dilutes emission rates over the  
29 grid cells. The resolution effect is the lowest at background stations, which are not  
30 influenced by any single source, but rather by the integrated contribution from all  
31 sources upwind of the stations where variations are less than 1% for O<sub>3</sub> and PM<sub>10</sub> (< 1

1  $\mu\text{gm}^{-3}$ ). However, background  $\text{NO}_2$  levels increase by  $\sim 1 \mu\text{gm}^{-3}$  (48%) from 4 km to 1  
2 km.

3 [Figure 10](#) shows the temporal series and daily cycles for  $\text{NO}_2$  and  $\text{O}_3$  at traffic and  
4 background stations throughout the episode of 12-18<sup>th</sup> April, 2013. At traffic stations,  
5 the temporal series show a remarkable  $\text{O}_3$  daily cycle (observed 25p =  $23.2 \mu\text{gm}^{-3}$  and  
6 75p =  $77.5 \mu\text{gm}^{-3}$ ), due to  $\text{O}_3$  destruction caused by high  $\text{NO}_x$  levels (observed 50p =  
7  $34.5 \mu\text{gm}^{-3}$ ). In contrast, the  $\text{NO}_2$ -limited regime at background sites (observed 50p =  
8  $19 \mu\text{gm}^{-3}$ ) allows higher  $\text{O}_3$  concentrations (observed 25p =  $38 \mu\text{gm}^{-3}$  and 75p =  $89$   
9  $\mu\text{gm}^{-3}$ ) than in high  $\text{NO}_2$  environments.

10 During the episode mentioned above, the resolution increase at traffic stations had a  
11 positive effect by increasing the correlation coefficient for  $\text{NO}_2$  (from 0.73 to 0.76) and  
12  $\text{O}_3$  (from 0.83 to 0.86), and also by decreasing the  $\text{NO}_2$  mean bias by  $\sim 5 \mu\text{gm}^{-3}$  (from 6  
13 to  $1 \mu\text{gm}^{-3}$ ). The  $\text{NO}_2$  daily cycle improves in the morning hours after sunrise, reducing  
14 bias by  $5\text{-}10 \mu\text{gm}^{-3}$  and contributing to a reduction in  $\text{O}_3$  overestimations ( $\sim 5 \mu\text{gm}^{-3}$ ). In  
15 contrast, at background stations, where the  $\text{NO}_x/\text{O}_3$  chemistry is less dominant, the  
16 resolution effect is not significant. Such behavior indicates that finer resolution  
17 improves the performance, because horizontal resolution affects the representation of  
18 chemical processes near large emission sources, such as the efficient formation of  $\text{O}_3$   
19 and nighttime  $\text{O}_3$  titration ([Mathur et al., 2005](#)). However, the loss of subgrid variability  
20 and improved meteorological fields (transport and temperature) are required.

## 21 **5 Conclusions**

22 The present work shows the effects of increasing the horizontal resolution from 4 km to  
23 1 km using the CALIOPE-AQFS on pollutant concentrations ( $\text{NO}_2$ ,  $\text{O}_3$ , and  $\text{PM}_{10}$ ) over  
24 three Spanish domains (AND, BCN and MAD) in April 2013.

25 The global features of concentration maps at both resolutions are quite similar, with  
26 zones of high/low concentration identically located, which is obviously because both  
27 simulations are based on the same emission dataset. Further comparisons demonstrate  
28 that increasing the resolution provides better-defined and more realistic concentration  
29 structures over large sources (roads and industries) and complex terrains (more sharply  
30 defined orographic hills). The titration effect on  $\text{O}_3$  concentrations along highways and  
31 major point sources is more evident in 1-km simulations than at 4 km, because the latter

1 is affected by higher dilution within the grid cells. This improvement is quantified by an  
2 increase in spatial correlation coefficients of 3% (6%) for NO<sub>2</sub> (O<sub>3</sub>).

3 However, the resolution increase in the range of 4-1 km does not exhibit the expected  
4 improvement in hourly statistics for any pollutant. Hourly correlation coefficients do  
5 not significantly change, and absolute (relative) errors and biases vary < 2 μgm<sup>-3</sup> (9%).  
6 The merit of the resolution increase may be underrated when classical statistics are  
7 applied at measurement stations (Mass et al., 2002; Gego et al., 2005). For instance,  
8 although the structure of important NO<sub>2</sub> urban plume features (> 40 μgm<sup>-3</sup>) often  
9 become more realistic (stronger and more defined plumes) as resolution increases,  
10 statistics are deeply degraded by even small timing and spatial errors.

11 The resolution increase has a significant impact on reducing NO<sub>2</sub> hourly bias (by 42%,  
12 2 μgm<sup>-3</sup>), without any significant change in the error and the r (<2%), but it increases O<sub>3</sub>  
13 hourly biases (<1 μgm<sup>-3</sup>). The main differences between resolutions appear at daytime  
14 and nighttime traffic peaks, when the mixing height experiences rapid changes,  
15 allowing the 1-km simulation to slightly reduce NO<sub>2</sub> underestimation in the morning by  
16 ~5-10 μgm<sup>-3</sup>. The O<sub>3</sub> daily cycles at large sources depict a high influence of hourly NO<sub>2</sub>  
17 concentrations, increasing the hourly O<sub>3</sub> bias by ~3 μgm<sup>-3</sup>. That behavior is controlled  
18 by the daytime O<sub>3</sub> underestimation and, to a lesser extent, by the nighttime  
19 overestimation. The resolution increase allows reducing the O<sub>3</sub> overestimations at night  
20 (by ~5 μgm<sup>-3</sup>), partly because of higher nocturnal NO<sub>2</sub> concentrations.

21 Concerning the capability of forecasting 75p exceedances in the observed maximum 1h  
22 concentrations, the increased resolution has a positive effect: it increases the number of  
23 hits that forecast 75p exceedances in the observed Max 1h NO<sub>2</sub> (537 vs. 466 over 953  
24 exceedances), and it reduces the false alarms for Max 1h O<sub>3</sub> exceedances (FAR  
25 improves by 37%).

26 The grid effect is less pronounced for PM<sub>10</sub> than for NO<sub>2</sub> and O<sub>3</sub>. When the resolution  
27 increases, the low increment of PM<sub>10</sub> mean concentrations (<0.1 μgm<sup>-3</sup>) is the result of  
28 compensating biases of PM<sub>10</sub> components, which is controlled mainly by the PPM and  
29 EC increase as well as the SS decrease.

30 BCN is the domain where the resolution increase has the highest effect, with changes in  
31 bias (error) of 16-73% (< 5%), followed by AND with 4-43% (< 5%) and MAD < 3-5%

1 (< 1%). In BCN, as in the western Mediterranean Basin, the transport of O<sub>3</sub> and its  
2 precursors is governed by mesoscale circulation. In that sense, the resolution increase  
3 has a great impact over BCN, where induced mesoscale phenomena control the air flow;  
4 meanwhile synoptic transport is more prominent in MAD and AND. The benefits of  
5 increasing the resolution to 1 km over rural areas (Mass et al., 2002) are that it increases  
6 the accurate representation of mesoscale meteorological structures such as orographic  
7 wind and circulation. Over urban areas along the western Mediterranean coast (Toll and  
8 Baldasano, 2002; Jiménez et al., 2006; Fay and Neunhäuserer, 2006), further  
9 improvements and urbanization steps are required before seeing any benefits in  
10 increasing the resolution to 1 km.

11 In urban areas or near large emission sources (industrial and traffic stations), NO<sub>2</sub> and  
12 O<sub>3</sub> concentrations are more sensitive to changes in the grid resolution. The  
13 concentration increase in primary anthropogenic pollutants (NO<sub>2</sub>, PPM and EC) is  
14 obvious because the high resolution allows better allocation of emissions at point,  
15 linear and area sources. What is more, it decreases the artificial dilution of emissions  
16 when compared to the larger grid area. However, the 1-km simulation attempt to more  
17 accurately describe the chemical formation of O<sub>3</sub> and dilution of NO<sub>2</sub> concentrations  
18 over those areas was not generally successful.

19 This analysis demonstrates weaknesses in the current model formulations that cannot be  
20 resolved with only high-resolution modeling. The subgrid air quality variability at 1-km  
21 resolution is not reproduced over large emission sources or urban areas, because a finer  
22 spatial structure is expected but unresolved. There are some underlying problems. First,  
23 there is a loss of subgrid emission heterogeneity. Emission inputs to CTM are an  
24 average rate, which accounts for the volume averaged quantity of mass released per unit  
25 of time. No other information regarding emission allocation (e.g., point, linear or per  
26 area) is considered; for instance a large amount of mass can be emitted by a small  
27 portion of the grid surface or by several sources scattered around it (Galmarini et al.,  
28 2008; Cassiani et al., 2010; Ching and Majeed, 2012). Despite the fact that emissions  
29 are estimated by following a bottom-up approach emission model, emission  
30 heterogeneity is lost in the volume averaging process performed within CTM. The loss  
31 is even higher when resolution decreases (from 1 km to 4 km). Second, there is a low  
32 degree of complexity in flow and dispersion details at urban scales, where most of the  
33 pollutants come from street canyons and/or tree canopies, where they are transported

1 until mixing conditions allow the pollutants to disperse above these urban canopy levels  
2 ([Kim et al., 2013](#); [Ching, 2013](#)). Third, the USGS land-use data used in the WRF model  
3 is based on 1993 data, and urban changes in MAD and BCN over the last 20 years are  
4 significant.

5 Since temperature and wind speed are very sensitive to the ratio of building width to  
6 road width, the next improvement should focus on using an urban canopy model that  
7 considers effects on the transfer of energy and momentum between urban structures and  
8 the lower atmosphere. This is crucial for modeling meteorology and air quality.  
9 However, it requires an urban canopy scheme and a canopy parameter database (urban  
10 fraction, building height and area). Furthermore, in order to gain any benefits from  
11 increasing resolution, the meteorological modeling should include an improved  
12 description of the land instead of relying on USGS data from the year 1993. To this end,  
13 the Coordination of Information on the Environment (CORINE) provides a high  
14 resolution (100 m) land use database, which was developed by the European  
15 Environmental Agency and updated to the year 2006 (CLC2006) (EEA, 2007). This  
16 could be implemented in the WRF model following the methodology described in  
17 [Pineda et al. \(2004\)](#).

18

19

20

21

22

23

24

25

26

27

28



1 **Appendix A**

2 Table A1. Definition of the discrete statistics used in the evaluation. Where  $C_m(x, t)$  and  
 3  $C_o(x,t)$  are the modeled and observed concentrations at a location (x) and time (t); N is  
 4 the number of pairs of data.  $\bar{C}_m$  and  $\bar{C}_o$  are the modeled and observed mean  
 5 concentrations over the whole period, respectively.

Statistic	Formula	
Mean bias	$MB = \frac{1}{N} \sum_{i=1}^N (C_m(x,t) - C_o(x,t))$	A1
Mean normalized bias error	$MNBE = \frac{1}{N} \sum_{i=1}^N \frac{(C_m(x,t) - C_o(x,t))}{C_o(x,t)} \cdot 100$	A2
Mean fractional bias	$MFB = \frac{1}{N} \sum_{i=1}^N \frac{(C_m(x,t) - C_o(x,t))}{(C_o(x,t) + C_m(x,t)) / 2} \cdot 100$	A3
Mean 3rror	$ME = \frac{1}{N} \sum_{i=1}^N  C_m(x,t) - C_o(x,t) $	A4
Mean normalized gross 3rror	$MNGE = \frac{1}{N} \sum_{i=1}^N \frac{ C_m(x,t) - C_o(x,t) }{C_o(x,t)} \cdot 100$	A5
Mean fractional error	$MFE = \frac{1}{N} \sum_{i=1}^N \frac{ C_m(x,t) - C_o(x,t) }{(C_m(x,t) + C_o(x,t)) / 2} \cdot 100$	A6
Root mean squared error	$RMSE = \sqrt{\frac{1}{N} \sum_{i=1}^N (C_m(x,t) - C_o(x,t))^2}$	A7
Correlation coefficient	$r = \frac{\sum_{i=1}^N (C_m(x,t) - \bar{C}_m)(C_o(x,t) - \bar{C}_o)}{\sqrt{\sum_{i=1}^N (C_m(x,t) - \bar{C}_m)^2} \sqrt{\sum_{i=1}^N (C_o(x,t) - \bar{C}_o)^2}}$	A8

6

7 Table A2. Definition of the categorical statistics used in the evaluation. Exceedance  
 8 analysis is based on a comparison with a fixed threshold concentration (T), where a is  
 9 the number of false alarms, b is the number of hits, c is the number of correct negatives,  
 10 and d is the number of misses.

Statistic	Formula	
Accuracy	$A = \left( \frac{b+c}{a+b+c+d} \right) \cdot 100$	A9
Bias	$B = \left( \frac{a+b}{b+d} \right) \cdot 100$	A10

---

Critical success index	$CSI = \left( \frac{b}{a+b+d} \right) \cdot 100$	A11
Probability of detection	$POD = \left( \frac{b}{b+d} \right) \cdot 100$	A12
False alarm ratio	$FAR = \left( \frac{a}{a+b} \right) \cdot 100$	A13

---

1

## 2 **Acknowledgements**

3 The Spanish administrations “Generalitat de Catalunya”, “Junta de Andalucía”, and  
4 “Comunidad de Madrid” are acknowledged for providing air quality measurements. The  
5 CALIOPE-AQFS team (G.Arévalo, K. Serradell, D. Carrió, M. Castrillo, A. Soret, S.  
6 Basart and S. Gassó) and F. Benincasa are also thanked for their technical support. This  
7 work is funded by the post-doctoral grant held by M.T. Pay in the Beatriu de Pinós  
8 programme (2011 BP-A 00427), Andalusian contract (NET838690), and the Severo  
9 Ochoa Program awarded by the Spanish Government (SEV-2011-00067).

## 1 **References**

- 2 Appel, K.W., Pouliot, G.A., Simon, H., Sarwar, G., Pye, H.O.T., Napelenok, S.L.,  
3 Akhtar, F., and Roselle, S.J.: Evaluation of dust and trace metal estimates from the  
4 Community Multiscale Air Quality (CMAQ) model version 5.0, *Geosci. Model Dev.*, 6,  
5 883-899, doi:10.5194/gmd-6-883-2013, 2013.
- 6 Baldasano, J. M., Cremades, L., and Soriano, C.: Circulation of Air Pollutants over the  
7 Barcelona Geographical Area in Summer, in: *Proceedings of Sixth European*  
8 *Symposium Physico-Chemical Behaviour of Atmospheric Pollutants*, Varese (Italy),  
9 18–22 October, 1993, Report EUR 15609/1 EN, 474–479, 1994.
- 10 Baldasano J.M, Jiménez-Guerrero, P., Jorba, O., Pérez, C., López, E., Güereca, P.,  
11 Martín, F., García-Vivanco, M., Palomino, I., Querol, X., Pandolfi, M., Sanz, M.J., and  
12 Diéguez, J.J.: CALIOPE: An operational air quality forecasting system for the Iberian  
13 Peninsula, Balearic Islands and Canary Islands- First annual evaluation and ongoing  
14 developments, *Adv. Sci. Res.* 2, 89-98, 2008.
- 15 Baldasano, J.M., Pay, M.T., Jorba, O., Gassó, S., and Jiménez-Guerrero, P.: An annual  
16 assessment of air quality with the CALIOPE modeling system over Spain, *Sci. Total*  
17 *Environ.*, 409, 2163-2178, 2011.
- 18 Basart, S., Pérez, C., Nickovic, S., Cuevas, E., and Baldasano, J.M.: Development and  
19 evaluation of the BSC-DREAM8b dust regional model over Northern Africa, the  
20 Mediterranean and the Middle East, *Tellus Series B – Chemical and Physical*  
21 *Meteorology*, 64, 1-12, 2012.
- 22 Byun, D. W. and Schere, K. L.: Review of the governing equations, computational  
23 algorithms and other components of the Models-3 Community Multiscale Air Quality  
24 (CMAQ) Modeling System, *App. Mech. Rev.* 59, 51-77, 2006.
- 25 Cassiani, M., Vinuesa, J.F., Galmarini, S., and Denby, B.: Stochastic fields method for  
26 sub-grid scale emission heterogeneity in mesoscale atmospheric dispersion models,  
27 *Atmos. Chem. Phys.*, 10, 267-277, 2010.
- 28 Ching, J.K.S., and Majeed, M.A.: An approach to characterized within-grid  
29 concentration variability in air quality models, *Atmos. Environ.*, 49, 348-360, 2012.

1 Ching, J.K.S.: A perspective on urban canopy layer modeling for weather, climate and  
2 air quality applications, *Urban Climate*, 3, 13-39, 2013.

3 CMAQ: Technical Documentation, Available at :  
4 [http://www.airqualitymodeling.org/cmaqwiki/index.php?title=CMAQ\\_version\\_5.0\\_%2](http://www.airqualitymodeling.org/cmaqwiki/index.php?title=CMAQ_version_5.0_%28February_2012_release%29_Technical_Documentation)  
5 [8February\\_2012\\_release%29\\_Technical\\_Documentation](http://www.airqualitymodeling.org/cmaqwiki/index.php?title=CMAQ_version_5.0_%28February_2012_release%29_Technical_Documentation), last access 8 January 2014.

6 Colette, A., Bessagnet, B., Meleux, F., Terrenoire, E., and Rouïl, L.: Frontiers in air  
7 quality modelling, *Geosci. Model Dev.*, 7, 203-210, 2014.

8 Cuvelier, C., Thunis, P., Karam, D., Schaap, M., Hendriks, C., Kranenburg, R., Fagerli,  
9 H., Nyíri, Á., Simpson, D., Wind, P., Schulz, M., Bessagnet, B., Colette, A., Terrenoire,  
10 E., Rouïl, L., Stern, R., Graff, A., Baldasano, J. M., and Pay, M. T.: ScaleDep:  
11 performance of European chemistry-transport models as function of horizontal spatial  
12 resolution, EMEP Report 1/2013, 63 pp., available at:  
13 [http://emep.int/publ/reports/2013/MSCW\\_technical\\_1\\_2013.pdf](http://emep.int/publ/reports/2013/MSCW_technical_1_2013.pdf), last access 4 April  
14 2013. Cohan, D.S., Hu, Y., and Russel, A.G.: Dependence of ozone sensitivity analysis  
15 on grid resolution, *Atmos. Environ.*, 40, 126-135, 2006.

16 Eder, B., Kang, D., Mathur, R., Yu, S., and Schere, K.: An operational evaluation of the  
17 Eta-CMAQ air quality forecast model, *Atmos. Environ.*, 40, 4894-4905, 2006.

18 EEA: CLC2006 technical guidelines. EEA Technical Report 17/2007. ISBN 978-90-  
19 9167-968-3. doi 10.2800/12134, 70 pp., 2007.

20 EEA: The application of models under the European Union's Air Quality Directive: A  
21 technical reference guide, EEA Technical report 10/2011, Publication Office of the  
22 European Union, Luxembourg, ISSN Technical report series 1725-2237, ISBN 978-92-  
23 9213-223-1, doi: 10.2800/80600, 76 pp., 2011.

24 EEA: Air quality in Europe- 2013 report, EEA Report 9/2013, ISSN 1725-9177, 112  
25 pp., 2013.

26 Fay, B. and Neunhäuserer, L.: Evaluation of high-resolution forecast with the non-  
27 hydrostatic numerical weather prediction model Lokal modell for urban air pollution  
28 episodes in Helsinki, Oslo and Valencia, *Atmos. Chem. Phys.*, 6, 2107-2128, 2006.

- 1 Fountoukis, C., Koraj, Dh., Denier van der Gon, H.A.C., Charalampidis, P.E., Pilinis,  
2 C., and Pandis, S.N.: Impact of grid resolution on the predicted fine PM by a regional 3-  
3 D chemical transport model. *Atmos. Environ.*, 68, 24-32, 2013.
- 4 Galmarini, S., Vinuesa, J.F., and Martilli, A.: Modeling the impact of sub-grid scale  
5 emission variability on upper-air concentration, *Atmos. Chem. Phys.* 8, 141-158, 2008.
- 6 Garber, W., Colosio, J., Grittner, S., Larssen, S., Rasse, D., Schneider, J. and Houssiau,  
7 M.: Guidance on the Annexes to Decision 97/101/EC on Exchange of Information as  
8 revised by Decision 2001/752/EC, Technical Report, European Commission, DG  
9 Environment, 2002.
- 10 García-Valero, J.A., Montávez, J.P., Jérez, S., Gómez-Navarro, J.J., Lorente-Plazas, R.,  
11 and Jiménez-Guerrero, P.: A seasonal study of the atmospheric dynamics over the  
12 Iberian Peninsula based on circulation types, *Theor. Appl. Climatol.*, 110, 219-310,  
13 2012.
- 14 Gego, E., Hogrefe, C., Kallos, G., Voudouri, A., Irwin, J., and Rao, S.T.: Examination  
15 of model predictions at different horizontal grid resolutions, *Environ. Fluid Mech.*, 5,  
16 63-85, 2005.
- 17 Gong, S.L.: A parameterization of sea-salt aerosol source function for sub- and super-  
18 micron particles, *J. Geophys. Res.*, 17, 197, 2003.
- 19 Guenther, A., Karl, T., Harley, P., Wiedinmyer, C., Palmer, P.I., and Geron, C.: 2006.  
20 Estimates of global terrestrial isoprene emissions using MEGAN (Model of Emissions  
21 of Gases and Aerosols from Nature), *Atmos. Chem. Phys.*, 6, 3181-3210, 2006.
- 22 Gonçalves, M., Jiménez-Guerrero, P., and Baldasano, J.M.: Contribution of atmospheric  
23 processes affecting the dynamics of air pollution in South-Western Europe during a  
24 typical summertime photochemical episode, *Atmos. Chem. Phys.*, 9, 849-864, 2009.
- 25 Guevara, M., Martínez, F., Arévalo, G., Gassó, S. and Baldasano, J.M.: An improved  
26 system for modelling Spanish emissions: HERMESv2.0, *Atmos. Environ.*, 81, 209-221,  
27 2013.
- 28 Jiménez, P., Jorba, O., Parra, R., and Baldasano, J.M.: Evaluation of MM5-  
29 EMICAT2002-CMAQ performance and sensitivity in complex terrains: High-resolution

1 application to the northeastern Iberian Peninsula, *Atmos. Environ.*, 40, 5056-5072,  
2 2006.

3 Kain, J.S. and Fritsch, J.M.: A one-dimensional entraining/detraining plume model and  
4 its application in convective parameterization, *J. Atmos. Sci.*, 47 (23), 2784-2802, 1990.

5 Kang, D., Eder, B.K., Stein, A.F., Grell, G.A., Peckham, S.E., and McHenry, J.: The  
6 new England air quality forecasting pilot program: development of an evaluation  
7 protocol and performance benchmark, *J. Air Waste Manage. Assoc.*, 55, 1782-1796,  
8 2005.

9 Kim, Y., Sartelet, K., Raut, Jean-Christophe, and Chazette, P.: Evaluation of the  
10 weather research and forecast/urban model over Greater Paris, *Boundary-Layer  
11 Meteorol.*, 149(1), 105-132, 2013.

12 Makar, P. A., Gravel, S., Chirkov, V., Strawbridge, K. B., Froude, F., Arnold, J., and  
13 Brook, J.: Heat flux, urban properties, and regional weather, *Atmos. Environ.*, 40,  
14 2750–2766, 2006.

15 Mathur, R., Shankar, U., Hanna, A.F., Odman, M.T., McHenry, J.N., Coats, C. J.,  
16 Alapaty, K., Xiu, A., Arunachalam, S., Olerud Jr., D. T., Byun, D. W., Schere, K. L.,  
17 Binkowski, F. S., Ching, J. K. S., Dennis, R. L., Pierce, T. E., Pleim, J. E., Roselle, S.  
18 J., and Young, J. O.: Multiscale Air Quality Simulation Platform (MAQSIP): Initial  
19 applications and performance for tropospheric ozone and particulate matter, *J. Geophys.  
20 Res.*, 110 (D13308), doi:10.1029/2004JD004918, 2005.

21 Mass, C., Ovens, D., Albright, M., and Westrick, K.: Does increasing Horizontal  
22 resolution Produce better Forecasts? The results of two years of Real-time Numerical  
23 Weather prediction in the Pacific Northwest, *B. Am. Meteorol. Soc.*, 83, 407-430, 2002.

24 Millán, M., Salvador, R., Mantilla, E., and Kallos, G.: Photooxidant dynamics in the  
25 Mediterranean basin in summer: results from European research projects, *J. Geophys.  
26 Res.*, 102, 8811– 8823, 1997.

27 Pay, M.T., Jiménez-Guerrero, P., and Baldasano, J.M.: Implementation of resuspension  
28 from paved roads for the improvement of CALIOPE air quality system in Spain, *Atmos.  
29 Environ.*, 45, 802-807, 2011.

1 Pay, M.T., Jiménez-Guerrero, P., Jorba, O., Basart, S., Pandolfi, M., Querol, X., and  
2 Baldasano, J.M.: Spatio-temporal variability of levels and speciation of particulate  
3 matter across Spain in the CALIOPE modeling system, *Atmos. Environ.*, 46, 376-396,  
4 2012a.

5 Pay, M. T., Gassó, S., and Baldasano, J.M.: Evaluation of the CMAQ5.0 in the  
6 framework of the CALIOPE air quality forecasting system over Europe, in: 11<sup>th</sup> Annual  
7 CMAS Conference, Chapel Hill, North Carolina, USA, 15-17 October 2012, 2012b.

8 Pérez, C., Nickovic, S., Baldasano, J.M., Sicard, M., Rocadenbosch, F., and Cachorro,  
9 V.E.: A long Saharan dust event over the western mediterranean: Lidar, sun photometer  
10 observations, and regional dust modeling, *J. Geophys. Res.* 111 (D15214), 1-16, 2006.

11 Pineda, N., Jorba, O., Jorge, J., and Baldasano, J.M.: Using NOAA AVHRR and SPOT  
12 VGT data to estimate surface parameters: application to a mesoscale meteorological  
13 model, *Int. J. Remote Sens.* 25, 129–143, 2004.

14 Queen, A. and Zhang, Y.: Examining the sensitivity of MM5-CMAQ predictions to  
15 explicit microphysics schemes and horizontal grid resolutions, Part III - the impact of  
16 horizontal grid resolution, *Atmos. Environ.*, 42, 3869-3881, 2008.

17 San José, R., Pérez, J.L., Morant, J.L., and González Barras, R.M.: The use of Modern  
18 third-generation air quality models (MM5-EMIMO-CMAQ) for real-time operational  
19 air quality impact assessment of industrial plants, *Water Air Soil Pollu.*, 9, 27-37, 2009.

20 Skamarock, W.C., and Klemp, J.B.: A time-split nonhydrostatic atmospheric model for  
21 weather research and forecasting applications, *J. Comput. Phys.* 227 (7), 3465-3485,  
22 doi:10.1016/j.jcp.2007.01.037, 2008.

23 Szopa, S., Foret, G., Menut, L., and Cozic, A.: Impact of large scale circulation on  
24 European summer surface ozone and consequences for modelling forecast, *Atmos.*  
25 *Environ.*, 43, 1189-1195, 2009.

26 Thompson, T.M., Saari, R.K., and Selin, N.E.: Air quality resolution for health impacts  
27 assessment: influence of regional characteristics, *Atmos. Chem. Phys. Discuss.*, 13,  
28 14141-14161, doi:10.5194/acpd-13-14141-2013, 2013.



1 Tesche, T.W., Morris, R., Tonnesen, G., McNally, D., Boylan, J., and Brewer, P.:  
2 CMAQ/CAMx annual 2002 performance evaluation over the eastern US, *Atmos.*  
3 *Environ.* 40, 4906-4919, 2006.

4 Timmermans, R.M.A., Denier van der Gon, H.A.C., Kuenen, J.J.P., Segers, A.J.,  
5 Honoré, C., Perrussel, O., Builtjes, P.J.H., and Schaap, M.: Quantification of the urban  
6 air pollution increment and its dependency on the use of down-scaled and bottom-up  
7 city emission inventories, *Urban Climate*, 6, 44-62, 2013.

8 Toll, I. and Baldasano, J. M.: Modeling of photochemical air pollution in the Barcelona  
9 area with highly disaggregated anthropogenic and biogenic emissions, *Atmos. Environ.*,  
10 34, 3060– 3084, 2000.

11 Valari, M. and Menut, L.: Does an increase in air quality models' resolution bring  
12 surface ozone concentrations closer to reality?, *J. Atmos. Oceanic Technol.*, 25, 1955-  
13 1968, 2008.

14 Valverde, V. V., Pay, M. T., and Baldasano, J. M.: Climatic synoptic classification over  
15 the Iberian Peninsula oriented to air quality dynamic characterization, *Int. J. Climatol.*,  
16 submitted, 2014.

17 Vivanco, M., Correa, M., Azula, O., Palomino, I., and Martín, F.: Influence of model  
18 resolution on ozone predictions over Madrid area (Spain), in: *Computational Science*  
19 *and Its Applications–ICCSA 2008* (pp. 165-178), Springer Berlin Heidelberg, 2008.

20 WHO: Review of evidence on health aspects of air pollution – REVIHAAP Project  
21 Technical report, World Health Organization, Regional Office for Europe, Copenhagen,  
22 Denmark, 2013.

23 Yarwood, G., Roa, S., Yocke, M., and Whitten, G.: Updates to the carbon bond  
24 chemical mechanism: CB05, Final report to the US EPA, RT-0400675, 2005.

25 Zhang, K., Knipping, E., Wexler, A., Bhave, P., and Tonnensen, G.: Size distribution of  
26 sea-salt emissions as a function of relative humidity, *Atmos. Environ.*, 39, 3373-3379,  
27 2005.

1 Zhang, Y., Bocquet, M., Mallet, V., Seigneur, C., and Baklanov, A.: Real-time air  
2 quality forecasting, part I: History, techniques, and current status, *Atmos. Environ.*, 60,  
3 632-655, 2012.

4

1 Table 1. CALIOPE-AQFS computational requirements, in terms of Central Processor  
 2 Units (CPU) and computational time (in min), for simulating 48h air quality forecasts as  
 3 a function of the domain: IP-4km (D2), AND-1km (D3), BCN-1km (D5) and MAD-  
 4 1km (D4), all of which are described in [Figure 1](#). D-domains are described in Figure 1.

	IP-4km (399x399 cells)	AND-1km (366x358 cells)	BCN-1km (146x146 cells)	MAD-1km (146x158 cells)
Meteorological Modeling	128 CPU/15 min	256 CPU/80 min	128 CPU/20 min	128 CPU/20 min
Emission Modeling	1 CPU/ 4 min	1 CPU/ 4 min	1 CPU/1 min	1 CPU/1 min
Air Quality modeling	256 CPU/210 min	256 CPU/220 min	128 CPU/150 min	128 CPU/110 min

5

6

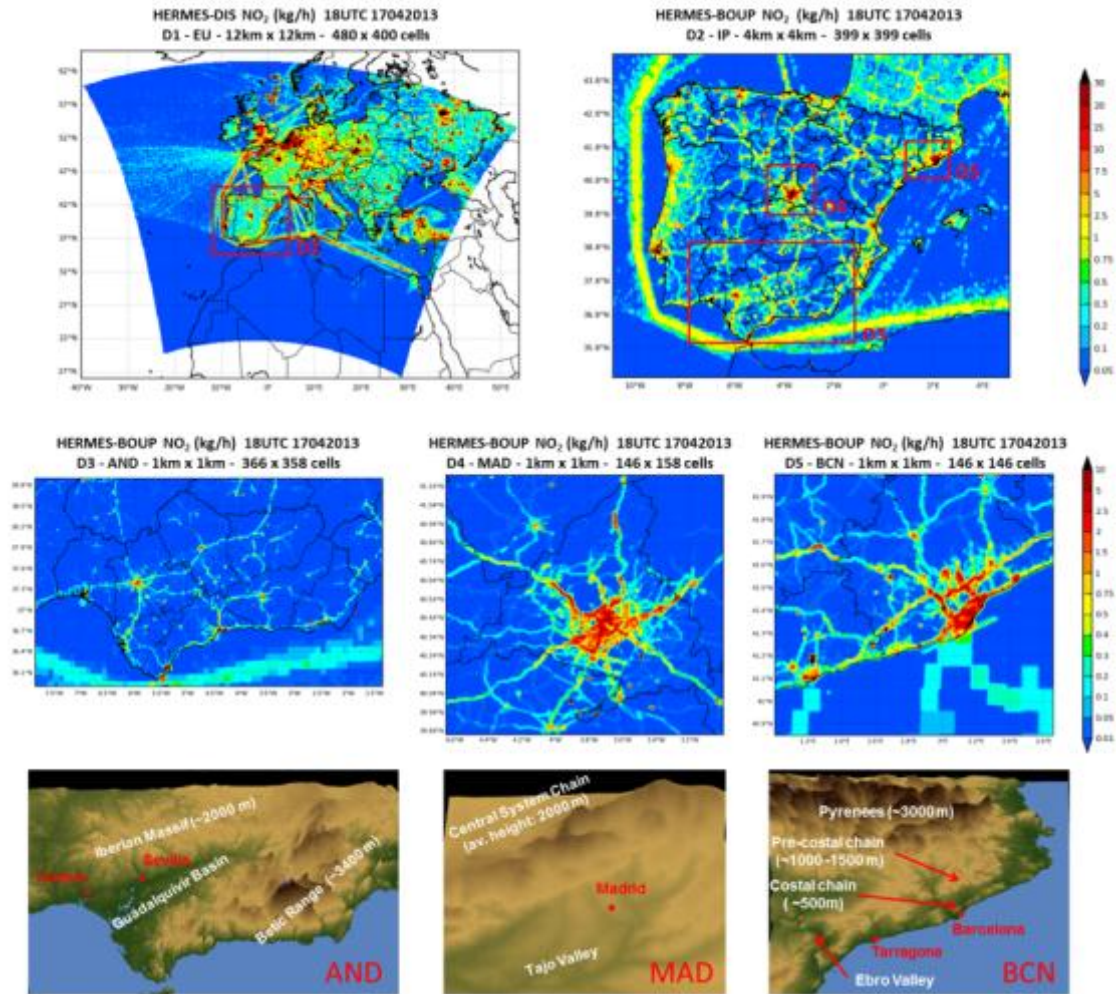
1 Table 2. Discrete and categorical statistics for NO<sub>2</sub>, O<sub>3</sub>, O<sub>3</sub>-8h, and PM<sub>10</sub> for April 2013  
 2 as a function of horizontal resolution (4 km and 1 km). n indicates the number of pairs  
 3 of data used in the discrete evaluation on an hourly basis. OM and MM depict the  
 4 measured and modeled mean concentrations, respectively. T is the threshold applied in  
 5 the categorical evaluation. Max 1h and mean 24h concentrations are calculated by  
 6 considering  $\geq 75\%$  of the hours in a day, as established by Directive 2008/50/EC.

	NO <sub>2</sub>		O <sub>3</sub>		O <sub>3</sub> -8h		PM <sub>10</sub>	
n (stations)	90761 (135)		76471 (114)		3248 (114)		66642 (100)	
OM ( $\mu\text{gm}^{-3}$ )	22.0		68.4		88.6		20.6	
EU LV/TV ( $\mu\text{gm}^{-3}$ ) (temp basis)	200 (Max 1h)		180 (Max 1h)		120 (Max 8h)		50 (Mean 24h)	
EU LV/TV exceedances	0		25		0		31	
T* ( $\mu\text{gm}^{-3}$ ) (temp. basis)	71 (Max 1h)		108 (Max 1h)		101 (Max 8h)		27 (Mean 24h)	
Discrete evaluation								
	4 km	1 km	4 km	1 km	4 km	1 km	4 km	1 km
MM ( $\mu\text{gm}^{-3}$ )	17.4	19.3	58.0	57.3	72.4	71.5	13.9	14.0
r	0.54	0.54	0.61	0.61	0.54	0.51	0.45	0.44
MB ( $\mu\text{gm}^{-3}$ )	-4.5	-2.6	-10.5	-11.3	-16.3	-17.2	-6.7	-6.6
MAE ( $\mu\text{gm}^{-3}$ )	12.9	13.2	19.7	19.8	18.4	19.2	12.6	12.7
RMSE ( $\mu\text{gm}^{-3}$ )	19.8	20.4	24.6	24.7	21.8	22.8	17.2	17.4
MNBE (%)	-20.4	-11.8	-15.3	-16.5	-18.4	-19.4	-32.5	-32.0
MNGE (%)	58.5	59.9	28.8	28.9	20.8	21.7	61.1	61.6
MFB (%)	-28.5	-23	-13.1	-15.1	-19.3	-20.5	-63.3	-64.1
MFE (%)	69.2	68.7	37.1	37.4	22.5	23.5	85.7	87.1
Categorical evaluation (Threshold = T*)								
	4 km	1 km	4 km	1 km	4 km	1 km	4 km	1 km
a (false alarm)	306	384	41	19	17	6	131	133
b (hits)	466	537	112	96	6	4	331	334
c (correct negative)	2517	2439	1846	1868	2826	2837	1978	1976
d (misses)	487	416	1194	1210	399	401	334	331
B (% , 100)	37	40	8	7	1	1	42	42
POD (% , 100)	49	56	9	7	1	1	50	50
CSI (% , 100)	81	97	12	9	6	2	69	70
FAR (% , 0)	40	42	27	17	74	60	28	28
A (% , 100)	79	79	61	62	87	87	83	83

T\* is defined as 75p of the observed concentrations estimated temporally, as established by EU Directive 2008/50/EC

7

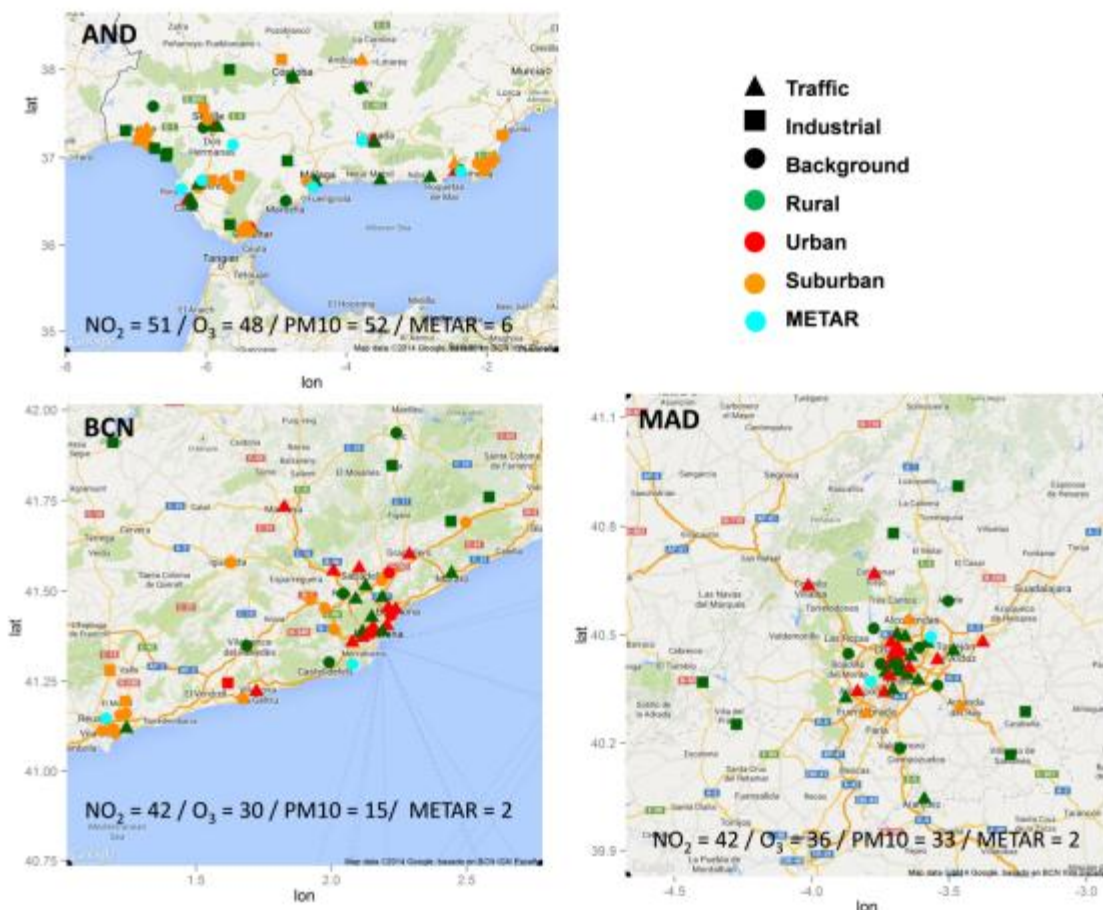
8



1

2 Fig. 1. CALIOPE-AQFS nesting strategy (D-domains) and study domains (Andalucia,  
 3 AND; Madrid, MAD; and Barcelona, BCN). Colour chart at D-domains shows NO<sub>2</sub>  
 4 emission rate (kg h<sup>-1</sup>) for 17<sup>th</sup> April, 2013 at 18UTC. HERMES-DIS model generates  
 5 emissions at 12 km x 12 km over Europe (the mother domain, D1) by performing  
 6 disaggregation from the EMEP database. HERMES-BOUP model estimates emissions  
 7 at 1 km x 1 km, following a bottom-up approach.

8

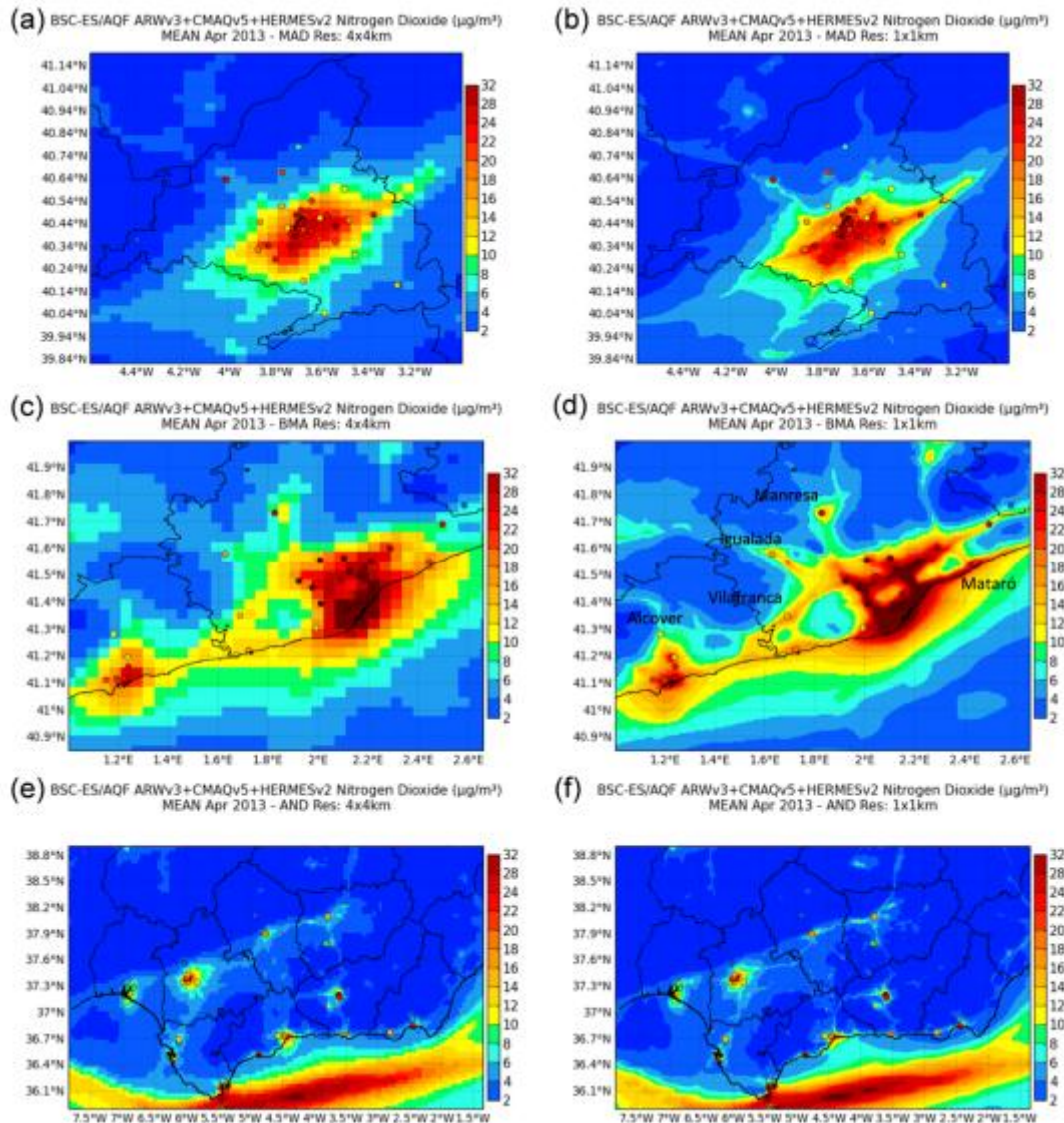


1

2 Figure 2. Air quality stations for  $\text{NO}_2$ ,  $\text{O}_3$  and  $\text{PM}_{10}$  in the three domains under study  
 3 (AND, BCN and MAD) in April 2013. Different types of stations are shown by symbols  
 4 and color codes. The various symbols represent the major emission type affecting each  
 5 station (Traffic: triangle; Industrial: square; and Background: circle), while the colors  
 6 reflect the environment of each station (Urban: red; Suburban: green; and Rural:  
 7 orange). Cyan dots represent METAR stations used in Sect. S1.

8

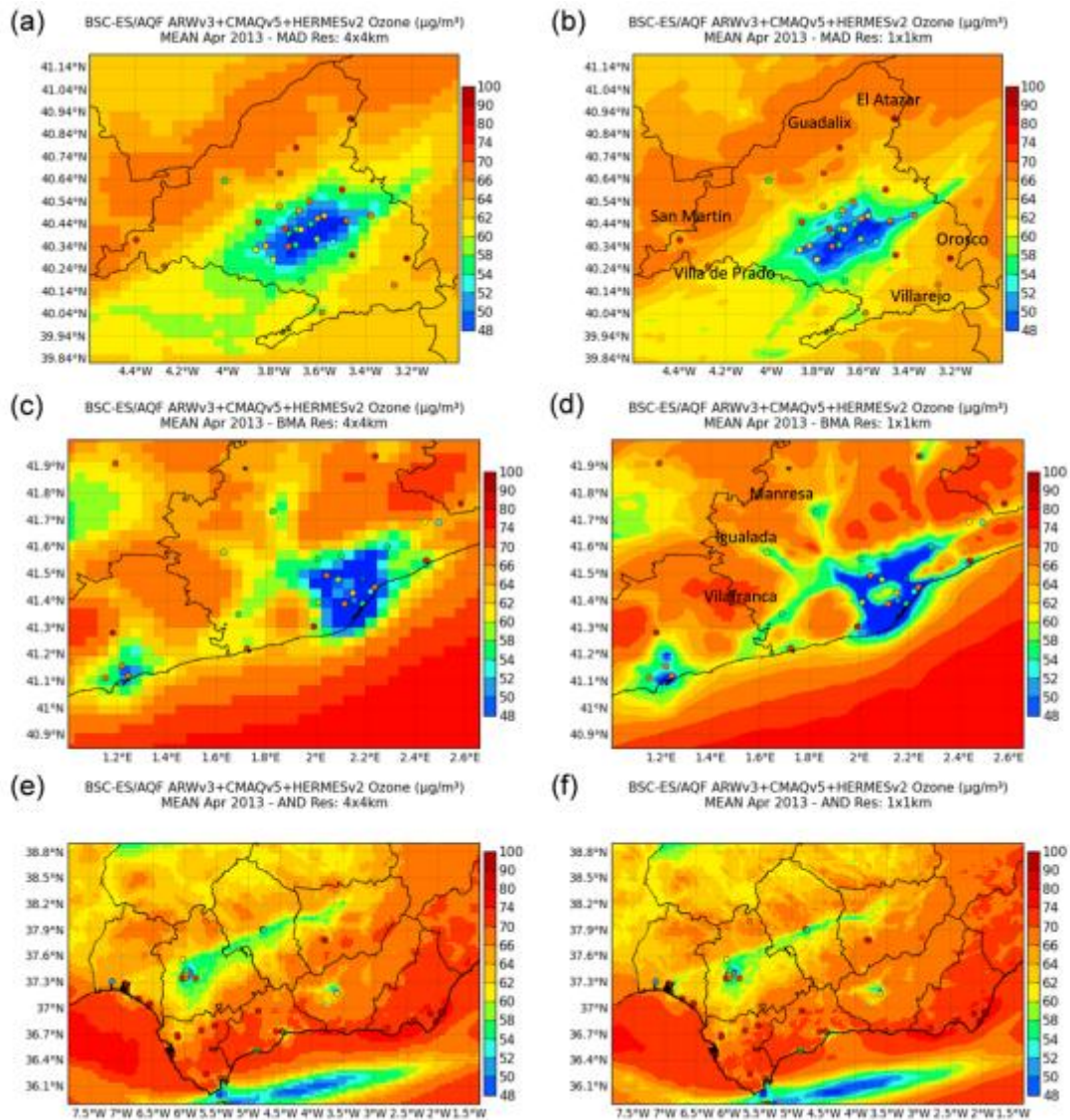




1

2 Figure 3. CALIOPE-AQFS mean NO<sub>2</sub> concentration ( $\mu\text{g}/\text{m}^3$ ) in April 2013 over (a,b)  
 3 MAD, (c,d) BCN, and (e,f) AND, as a function of horizontal resolution: 4 km (left  
 4 column) and 1 km (right column). Dots indicate mean concentration at air quality  
 5 stations.

6

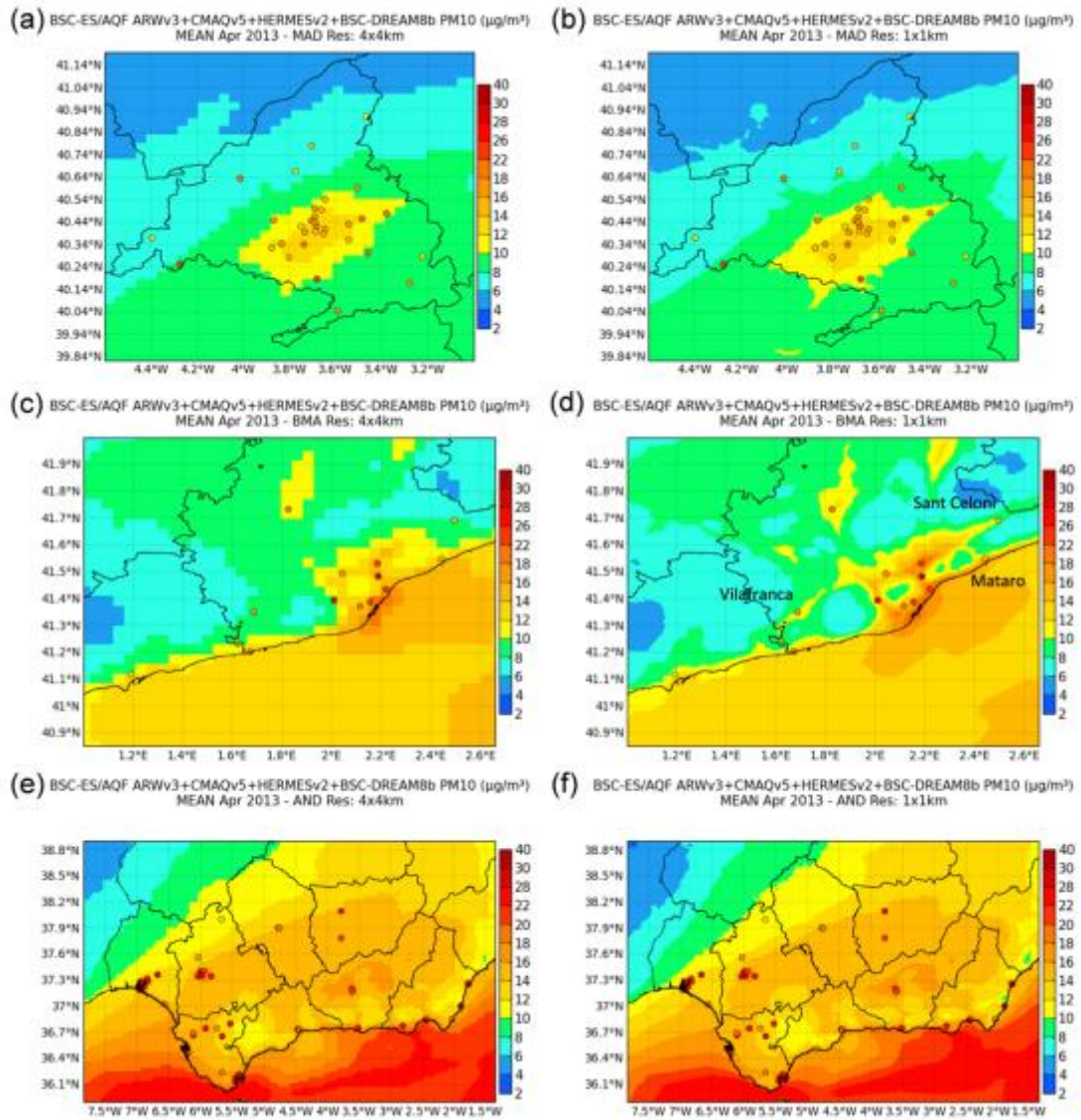


1

2 Figure 4. CALIOPE-AQFS mean O<sub>3</sub> concentration (µg<sup>-3</sup>) in April 2013 over (a,b)  
 3 MAD, (c,d) BCN, and (e,f) AND, as a function of horizontal resolution: 4 km (left  
 4 column) and 1 km (right column). Dots indicate mean concentration at air quality  
 5 stations.

6

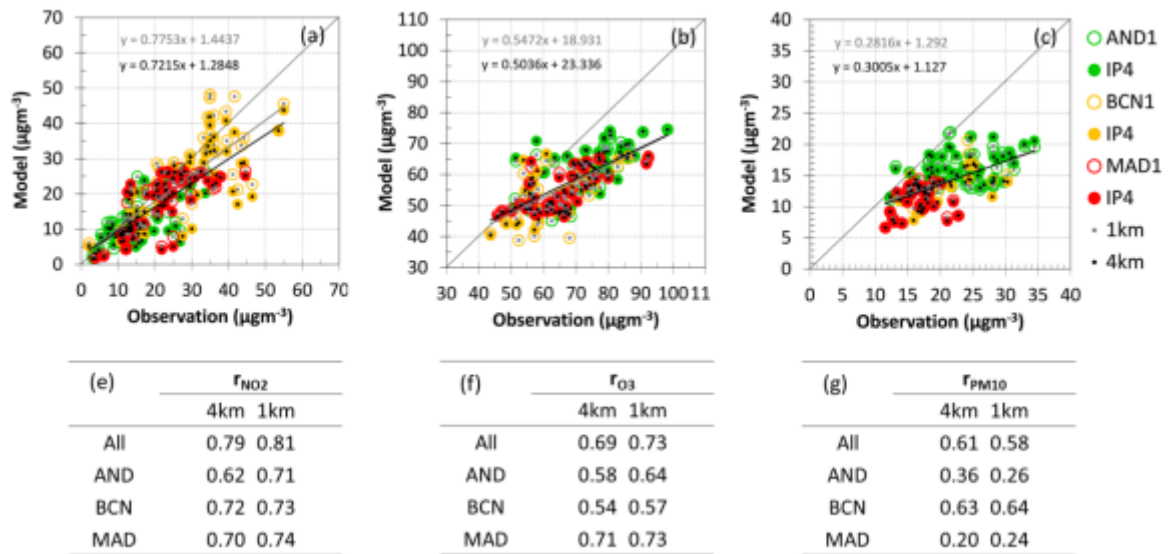




1

2 Figure 5. CALIOPE-AQFS mean  $\text{PM}_{10}$  concentration ( $\mu\text{g}/\text{m}^3$ ) in April 2013 over (a,b)  
 3 MAD, (c,d) BCN, and (e,f) AND, as a function of horizontal resolution: 4 km (left  
 4 column) and 1 km (right column). Dots indicate mean concentrations at air quality  
 5 stations.

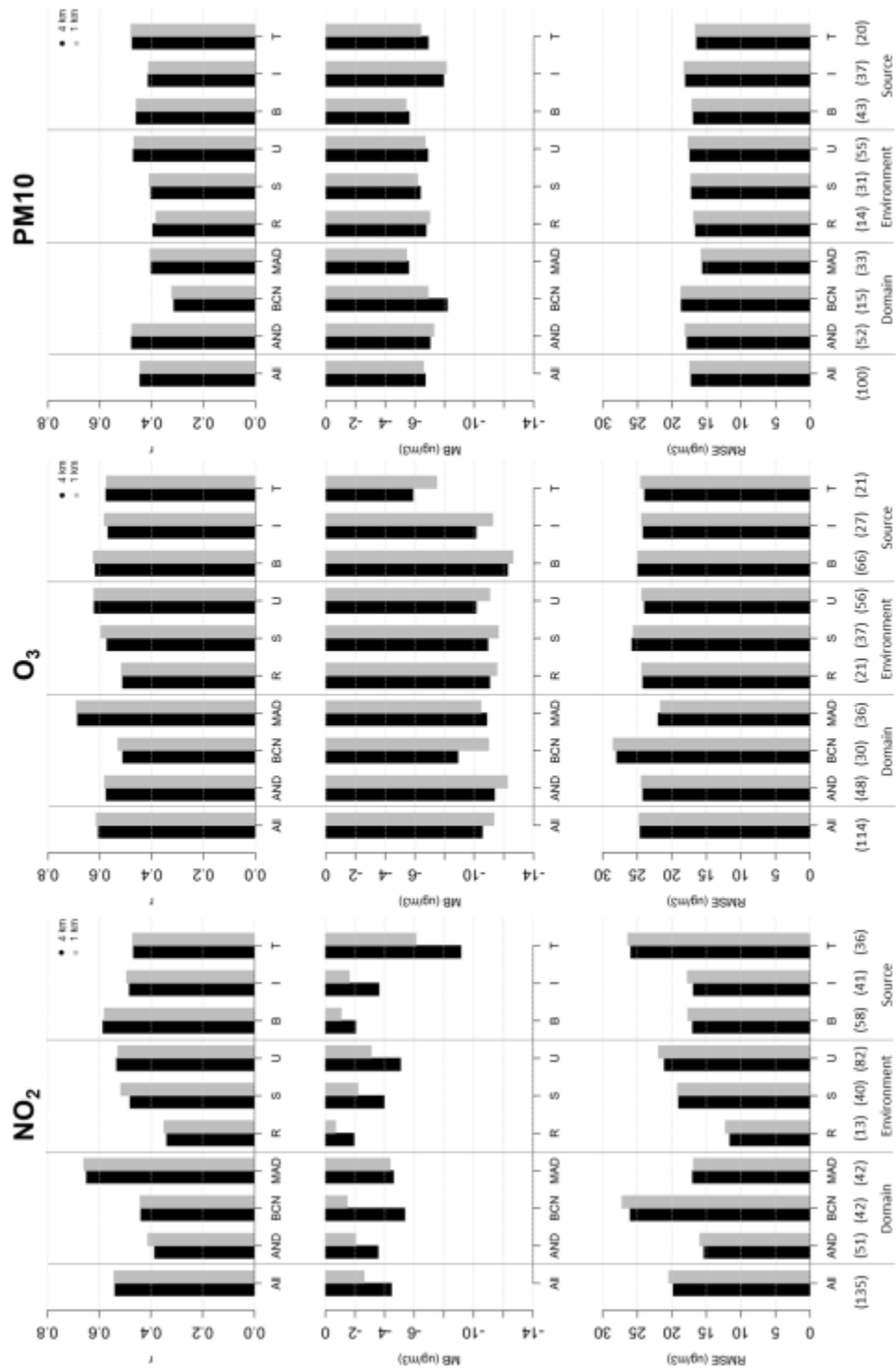
6



1

2 Figure 6. Monthly mean scatter plots for CALIOPE-AQFS (y-axis) and observed (x-  
 3 axis) concentrations for the three study domains (AND in green, BCN in yellow, and  
 4 MAD in red), as a function of horizontal resolution for (a) NO<sub>2</sub>, (b) O<sub>3</sub> and (c) PM<sub>10</sub>.  
 5 Equations show the linear adjustment between models and observations at 1 km (light  
 6 grey) and 4 km (dark grey). Spatial correlation coefficients as a function of resolution  
 7 and domain are shown for (e) NO<sub>2</sub>, (f) O<sub>3</sub>, and (g) PM<sub>10</sub>.

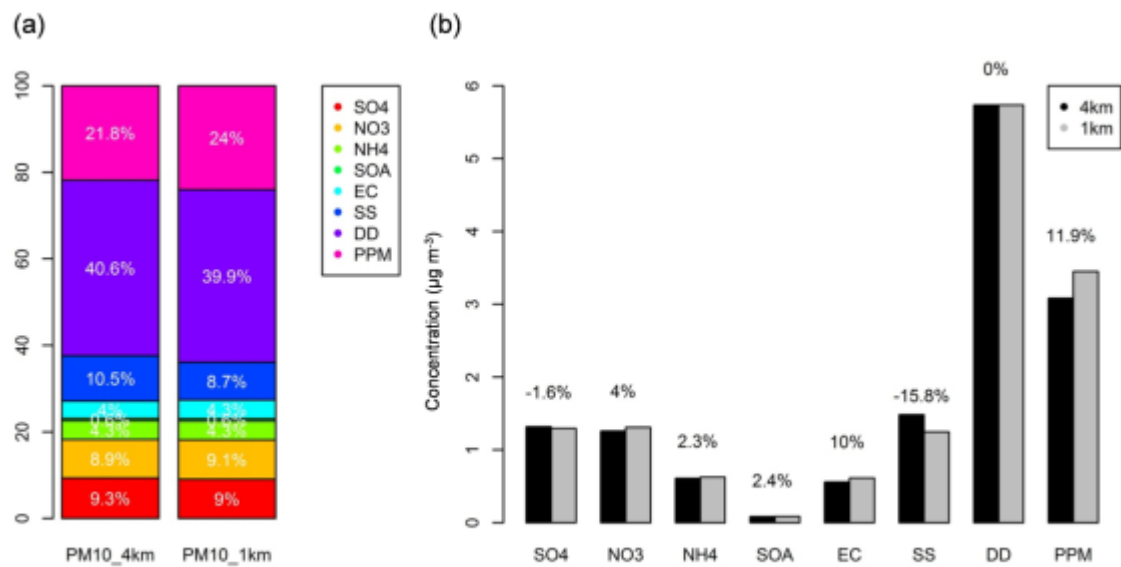
8



1

2 Figure 7. Statistics (r, MB, and RMSE in rows) for each pollutant ( $\text{NO}_2$ ,  $\text{O}_3$ , and  $\text{PM}_{10}$ )  
 3 in columns) on an hourly basis as a function of horizontal resolution: 4 km (black) and 1  
 4 km (grey). Four categories are considered: all stations (all), domain (AND, BCN and  
 5 MAD), station environment (R, S, and U), and main sources (B, I, and T).

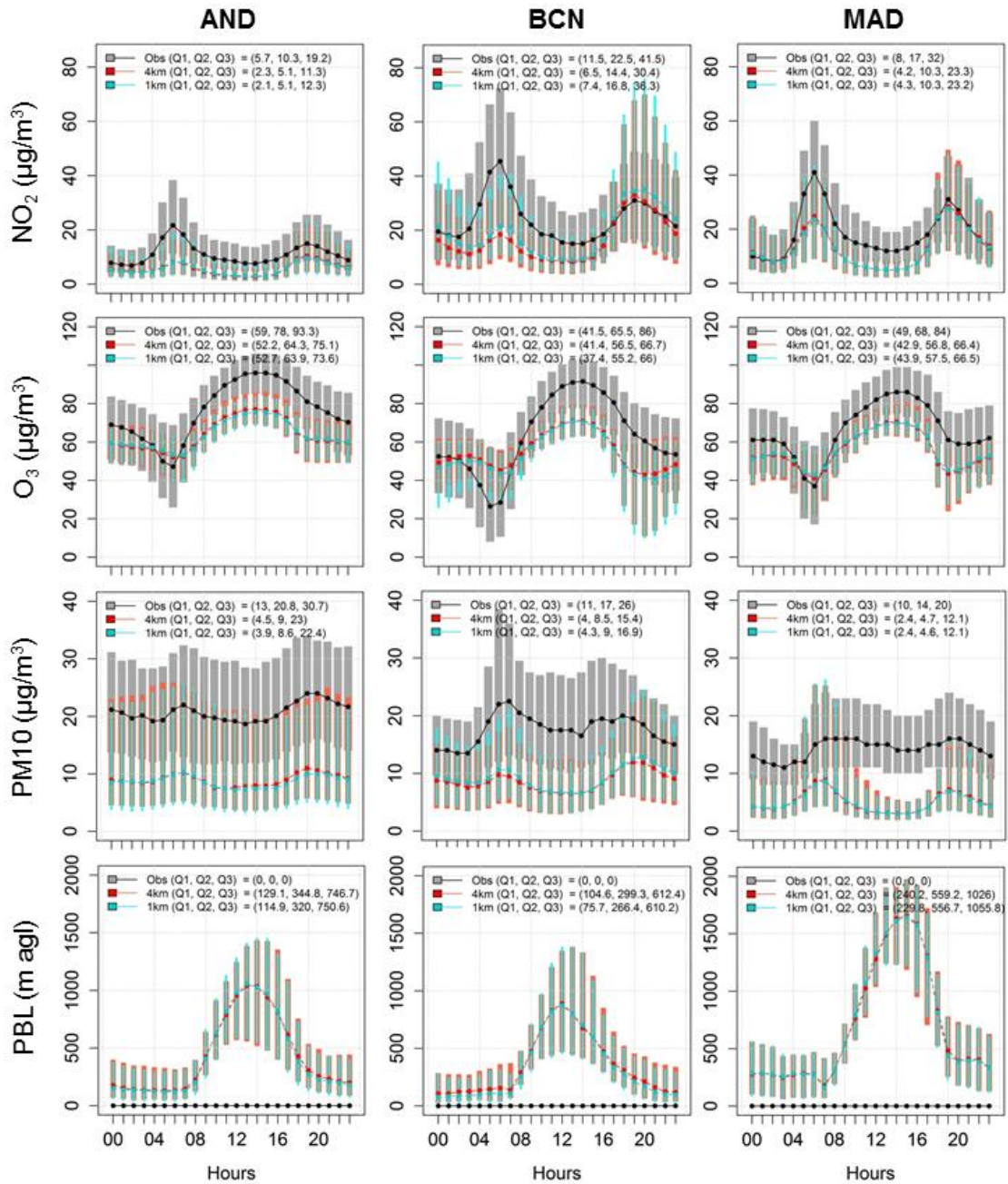
6



1

2 Figure 8. Resolution effect on PM<sub>10</sub> components in April 2013. (a) Percentage of PM<sub>10</sub>  
 3 components: sulfate (SO<sub>4</sub>), nitrate (NO<sub>3</sub>), ammonium (NH<sub>4</sub>), secondary organic  
 4 aerosol (SOA), elemental carbon (EC), sea salt (SS), desert dust (DD), and primary  
 5 particulate matter (PPM). (b) PM<sub>10</sub> component concentrations in the 1-km simulation  
 6 (black) and 4-km simulation (grey). Numbers over bars indicate the % of increase when  
 7 increasing resolution.

8

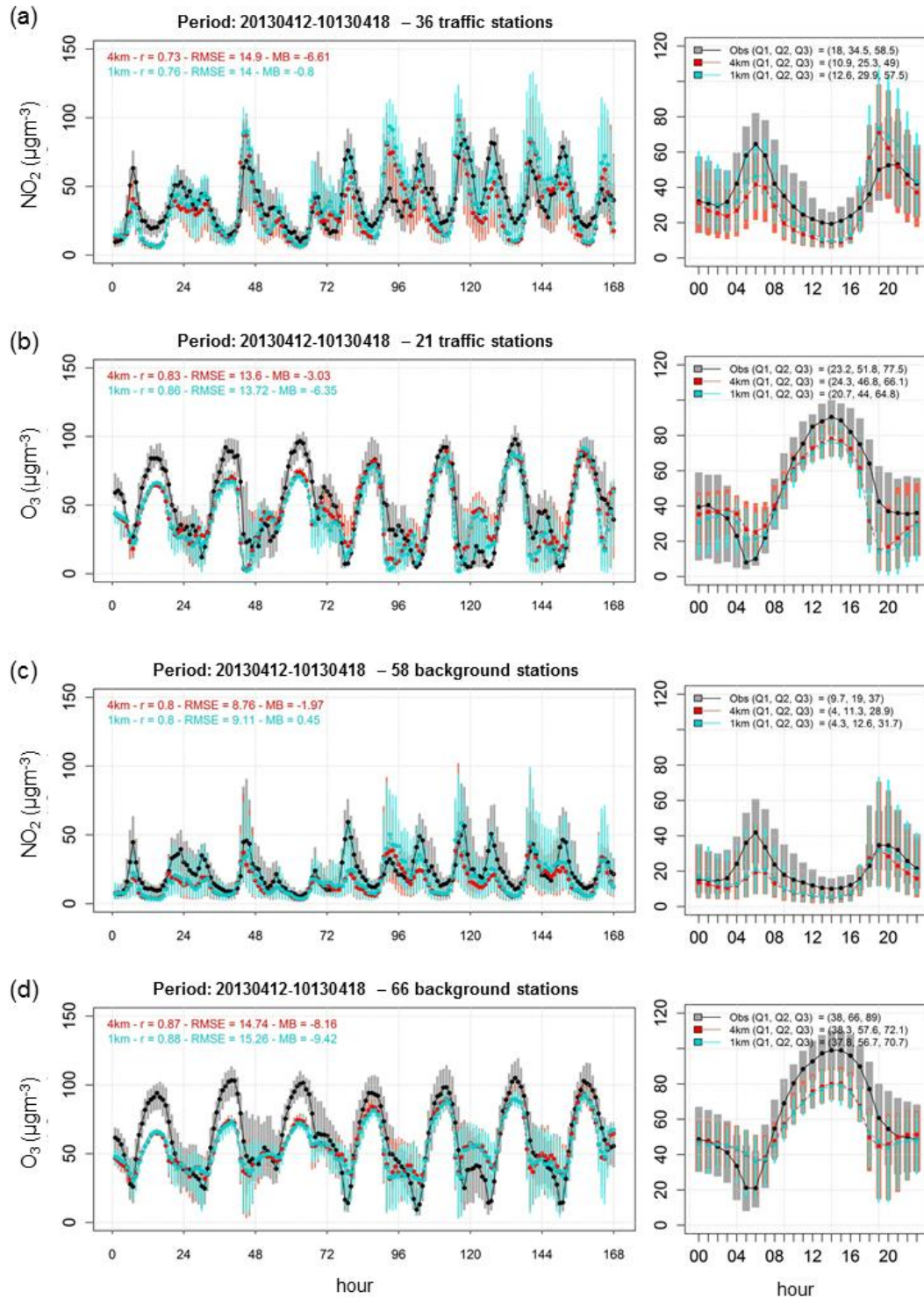


2

3 Figure 9. Daily cycles for  $\text{NO}_2$ ,  $\text{O}_3$  and  $\text{PM}_{10}$  for each study domain at available stations  
 4 as a function of resolution. No observations of PBL are available. Q1, Q2 and Q3  
 5 indicate quartiles for the daily cycle. Bars show Q1 and Q3 at each hour.

6





1

2 Figure 10. Temporal series and daily cycles for NO<sub>2</sub> and O<sub>3</sub> at background (a and b,  
 3 respectively) and traffic stations (c and d, respectively) for the episode of 12-18<sup>th</sup> April,  
 4 2013. Q1, Q2 and Q3 indicate quartiles for the daily cycle. Bars show Q1 and Q3 at  
 5 each hour.